

Article

Influence of Composite Thickness on Ultrasonic Guided Wave Propagation for Damage Detection Using Embedded PZT Transducers

Tianyi Feng  and M. H. Ferri Aliabadi * 

Structural Integrity and Health Monitoring Group, Department of Aeronautics, Imperial College London, South Kensington, London SW7 2AZ, UK; t.feng17@imperial.ac.uk

* Correspondence: m.h.aliabadi@imperial.ac.uk

Abstract: This paper describes a study that focuses on assessing the influence of composites with different thicknesses (2 mm, 4 mm, and 9 mm) on embedded ultrasonic guided waves (UGWs) under varying temperatures. The study also demonstrates the effectiveness of these embedded sensors in identifying damage. A novel cut-out method that included an embedded diagnostic layer and phased-array lead zirconate titanate (PZT) transducers, created using the ink-jet printing technique in the manufacturing process was employed. The research then focused on studying the behavior of UGWs under varying temperatures for each composite panel. This analysis aimed to understand how temperature variations affected the propagation of guided waves in thick composites. Finally, artificial damage on the surface and impact damage were introduced, both embedded and surface-mounted PZT transducers were used to detect and locate these damages in different thickness composite panels. The results of damage localization indicated that the embedded PZT transducers were more sensitive than the surface-mounted transducers in locating the damage in thick composites.

Keywords: structural health monitoring (SHM); embedded lead zirconate titanate (PZT) transducers; thickness influences; thick composites; damage detection and localization



Citation: Feng, T.; Aliabadi, M.H.F. Influence of Composite Thickness on Ultrasonic Guided Wave Propagation for Damage Detection Using Embedded PZT Transducers. *Appl. Sci.* **2023**, *13*, 10474. <https://doi.org/10.3390/app131810474>

Academic Editor: Cecilia Surace

Received: 1 August 2023

Revised: 7 September 2023

Accepted: 13 September 2023

Published: 19 September 2023



Copyright: © 2023 by the authors. Licensee MDPI, Basel, Switzerland. This article is an open access article distributed under the terms and conditions of the Creative Commons Attribution (CC BY) license (<https://creativecommons.org/licenses/by/4.0/>).

1. Introduction

Barely visible impact damage (BVID) poses a significant threat to the structural integrity of carbon fiber-reinforced polymer (CFRP) composites, and its detection and mitigation are essential to ensure the safe and reliable performance of composite materials in various applications. Monitoring techniques and preventive measures play a critical role in addressing this challenge. Structural health monitoring (SHM) plays a vital role in this context by providing continuous monitoring, early detection of damage, and accurate evaluation of its severity [1–5]. Ultrasonic guided waves (UGWs) have proven to be sensitive and effective in detecting various types of damage in thin-walled CFRP composite structures [6–13]. These guided waves can propagate over longer distances with relatively lower attenuations compared to other wave modes [14–16]. For active UGW sensing, lead zirconate titanate (PZT) transducers are commonly used due to their durability and low power consumption [17]. Typically, these PZT transducers are surface-mounted on CFRP composites. However, they are susceptible to external environmental factors such as moisture, corrosion, and unforeseen impacts or loading, which can compromise their performance [18–20].

Moreover, when dealing with thick CFRP composite laminates, the sensitivity of UGWs actuated by surface-mounted PZT transducers may be limited for damage localization [21]. In such cases, considering the application of composite repair patches, it becomes highly desirable to have embedded PZT transducers for SHM [18]. Embedded PZT transducers offer several advantages, including improved durability of the transducers themselves and increased sensitivity for damage detection. Since embedded PZT

transducers are isolated from exposed environmental conditions, they experience reduced aging and maintain excellent stability, durability, and repeatability [18,22]. Therefore, it is necessary to embed PZT transducers into composites, especially for thick CFRP composites, to enhance the durability of the transducers and improve the sensitivity of UGWs for damage localization. Embedded PZT transducers not only address the limitations of surface-mounted transducers but also provide enhanced monitoring capabilities for structural health assessment in CFRP composites.

The study conducted by Dziendzikowski et al. [18] focused on comparing the A_0 mode of UGWs at 100 kHz, generated by both surface-mounted and embedded PZT transducers, for glass fiber-reinforced plastic (GFRP) composites. The researchers also investigated the electro-mechanical impedance (EMI) properties of the transducers and compared them. The EMI results revealed that the embedded PZT transducers exhibited a 50% higher coupling factor compared to the surface-mounted transducers in GFRP composites. This indicates that the embedded transducers had a more effective energy transfer between the transducer and the composite structure. The higher coupling factor suggests improved sensing capabilities for damage detection. In terms of signal-to-noise ratio (SNR), the study found that the embedded PZT transducers provided a better SNR compared to the surface-mounted transducers. A higher SNR indicates a stronger and clearer signal relative to the background noise, which enhances the detection capability of barely visible impact damage (BVID). BVID refers to damage that is not easily visible but can significantly affect the structural integrity of the composite. Additionally, the researchers utilized the damage localization RAPID algorithm to locate the BVID for different impact energies. The algorithm, combined with the embedded PZT transducers, allowed for accurate and reliable identification of the damage location, even for varying impact energies. This demonstrates the effectiveness of embedded PZT transducers in localizing and assessing BVID.

The study by Andreades et al. [23] proposed a novel embedding technique for PZT transducers in composite laminates. They utilized woven E-glass fiber fabric to provide electrical insulation for the top of the embedded transducers. The researchers found that artificial delamination and BVID could be detected using second harmonic generation and nonlinear modulation of the ultrasonic spectrum, employing a laser Doppler vibrometer (LDV). The results demonstrated that this novel embedding technique enables real-time ultrasonic inspection of carbon fiber-reinforced plastic (CFRP) composites. In another study by Dziendzikowski et al. [24] the detection and classification of surface-mounted artificial damage and BVID were investigated in GFRP composites with embedded PZT transducers. The researchers achieved a detection rate above 90% and an acceptable ratio of false-positive indications below 3%. These results indicate the feasibility of using embedded PZT transducers for damage detection in the early stages of SHM system development. Furthermore, Dziendzikowski et al. [24] proposed a novel Bayesian approach for damage classification. The Bayesian approach yielded a damage detection rate above 93% and a false rate below 3%. This suggests that the Bayesian approach is effective in accurately classifying different types of damage. Overall, this study demonstrates the effectiveness of embedded PZT transducers in detecting and classifying damage in composite structures. The novel embedding technique with electrical insulation and the utilization of advanced techniques such as second harmonic generation, nonlinear modulation, LDV, and Bayesian approaches contribute to the improved capabilities of the SHM system. These findings further support the potential of embedded PZT transducers for real-time ultrasonic inspection and reliable monitoring of composite structures.

In the field of embedding PZT transducers into composite laminates, two common methods are typically used: the direct insertion method [25–28] and the use of Stanford Multi-Actuator Receiver Transduction (SMART) Layer™ [2,29–31]. However, both methods have certain drawbacks that need to be addressed. The direct insertion method, while effective, can significantly increase the weight of the host structure due to the additional traditional wires used for connection [32]. On the other hand, the SMART Layer™ approach involves adding a relatively thick layer to the composite, which can contribute to its

degradation [32]. Moreover, during the manufacturing process, the exposed embedded circuits using above methods can affect the trim of the composites after curing, making it impractical for industrial fabrication and subsequent higher assembly steps.

To overcome these challenges, the authors presented a novel edge cut-out method [33] that involves embedding diagnostic films and phase-array PZT transducers into composites using inkjet printing techniques. This method offers several advantages over the traditional approaches. Firstly, the use of diagnostic films can reduce the weight of the extra cables by one-third [34]. Secondly, the active sensing capabilities of the embedded PZT transducers remain stable even after fatigue testing, ensuring long-term performance [35]. Additionally, the reduction in tensile and compressive modulus resulting from the embedding process remains acceptable, even in worst-case scenarios [35]. Furthermore, the diagnostic films used in this novel approach exhibit excellent performance during low- and high-temperature changes under cyclic loading, aligning with the operational and environmental conditions experienced by regional aircraft [36].

The author of this paper recently conducted a study on the thickness effect of UGWs by mounting diagnostic films with phased-array PZT transducers on the surface of CFRP composites [21]. However, the research mentioned in the previous discussions [21,33] did not specifically investigate the influence of thickness on ultrasonic guided waves (UGWs) and damage detection and localization using embedded PZT transducers in composite laminates. Building upon the author's previous work, this paper aims to provide an in-depth investigation into the influence of thickness on UGW propagation properties, as well as its impact on the reliability of damage detection and localization using embedded PZT transducers in composite laminates.

The primary objective of this paper is to explore how the thickness of the composite laminate can affect the propagation properties of embedded UGWs. By comparing the results obtained using surface-mounted PZT transducers from the author's previous work, the researchers aim to assess the impact of thickness on the reliability of damage localization. The study starts by employing active sensing techniques to analyze the guided wave propagation through composite panels with thicknesses of 2 mm, 4 mm, and 9 mm. This analysis considers how temperature variations impact the propagation behavior of UGWs within the composite panels. Finally, the paper focuses on damage detection and localization. The study aims to enhance our understanding of how thickness influences these factors, ultimately contributing to the advancement of structural health monitoring techniques for composite structures.

2. Experimental Setup

In the experiments conducted for this study, three composite panels were fabricated to investigate the effects of thickness on Lamb wave propagation in composites utilizing embedded PZT transducers. Unidirectional carbon fiber pre-pregs, specifically Hexply[®] IM7/8852 (Hexcel, Duxford, UK), were used for the lay-up process. The stacking sequences employed were quasi-isotropic, $[(0^\circ/+45^\circ/-45^\circ/+90^\circ)_n]_s$, with n representing the number of plies. The panel thicknesses manufactured are 2 mm, 4 mm, and 9 mm. The dimensions of the specimens were 300 mm \times 225 mm, and the average cured thicknesses for each composite panel were approximately 2 mm, 4 mm, and 9 mm, respectively. The embedding of PZT transducers was accomplished using DuraAct[™] (PI Ceramic GmbH, Lederhose, Germany) (P-876.K025) PZT transducers. Figure 1a illustrates the drawing of each composite panel, depicting the configuration of the PZT transducers. Additionally, Figure 1b provides a schematic representation of the diagnostic layers with embedded PZT transducers during the embedding process. These composite panels, along with the embedded PZT transducers, were specifically designed to investigate the thickness effects on Lamb wave propagation and enable a comparative analysis with the results obtained from surface-mounted PZT transducers in the author's previous work. The choice of material, lay-up configuration, and PZT transducers facilitates a systematic examination of the influence of thickness on Lamb wave behavior in composite laminates.

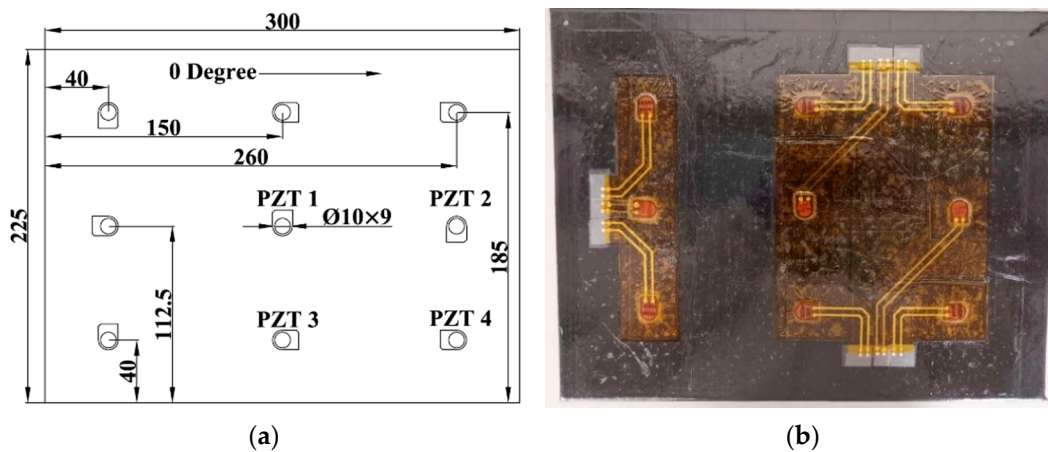


Figure 1. (a) Drawing of the composite panel; (b) schematic of embedded PZT transducers during lay-up.

Figure 2 shows the flow chart of the embedding technique for the composite manufacturing. To prepare the diagnostic layers with printed circuits, a Dimatix materials printer (DMP-2580) was utilized along with a silver-based ink containing nanoparticles at a concentration of 30–35 wt.%. The circuits were printed on Kapton® films (DuPont, Stevenage, UK), which had a thickness of 25.4 μm and a melting temperature of up to 400 °C. The piezo voltage for printing was set to 20 V, and a jetting frequency of 5 kHz ensured stable drop formation during the printing process. To achieve optimal printing quality, the substrate temperature was maintained at 55 °C, and a drop spacing of 35 μm was employed. To enhance the conductivity of the circuits and increase signal amplitudes, the circuits were printed three times with a width of 1.4 mm. After printing, the Kapton® films with the printed circuits were placed in a laboratory oven at 135 °C for 1 h to ensure the particles in the ink became conductive.

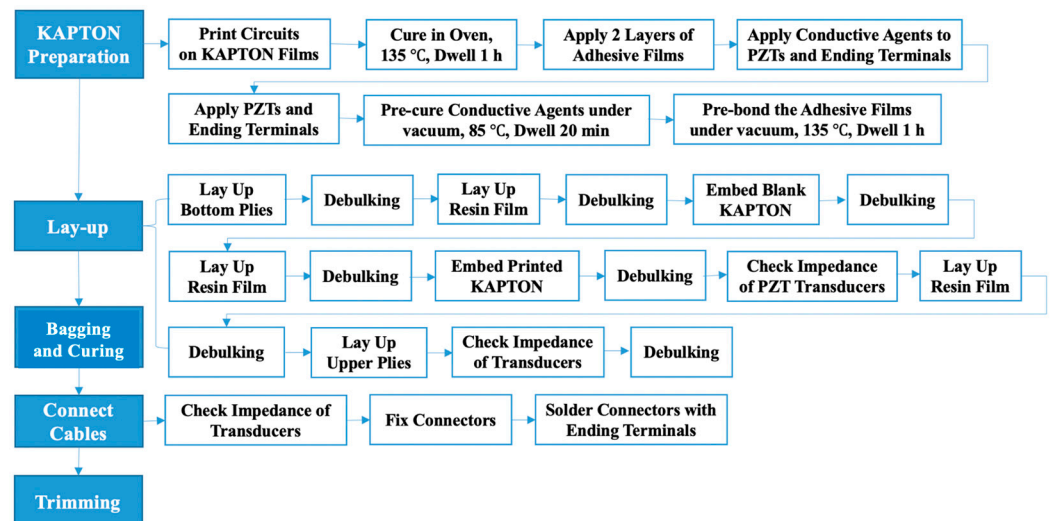


Figure 2. Flow chart of the manufacturing procedure.

Following the printing process, the nine PZT transducers needed to be connected and pre-bonded to the Kapton® films. In the author’s previous work [33], there were issues with connecting the circuits and connectors after the curing process, particularly at the cut-out position. The exposed printed circuits were prone to brittleness and damage, which led to the loss of connection for the embedded PZT transducers. This was a labor-intensive problem to resolve. Additionally, the conductive agents used for connecting the circuits and connectors required curing at 80 °C for 20 min, which was not a convenient method for

making connections. To address these challenges, high-temperature connecting terminals (Techni Measure Ltd., Doncaster, UK) (TML Co. TPF-2MS) were used. The terminals enabled soldering and ensured more stable connection quality when joining the circuits and connectors. Figure 3 provides an illustration of the high-temperature connecting terminals and their application in connecting the circuits and connectors.

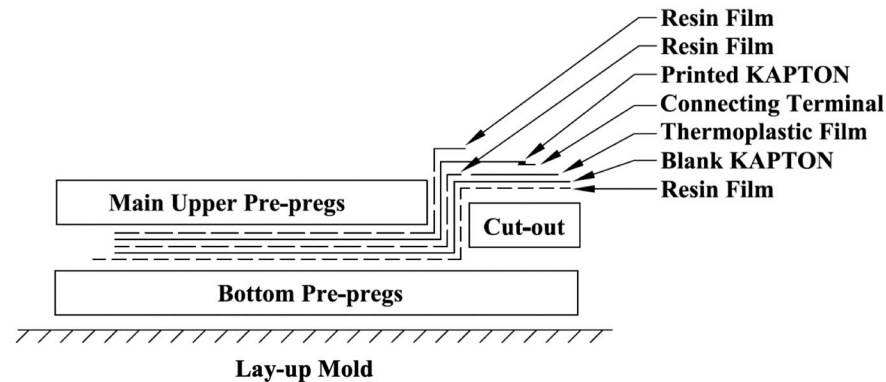


Figure 3. Schematic of cross-sectional part at cut-out position.

By implementing these high-temperature connecting terminals, the authors aimed to overcome the previous difficulties associated with connecting the printed circuits and connectors, leading to improved reliability and efficiency in the manufacturing process. To connect the PZT transducers and high-temperature connecting terminals, a small amount of conductive epoxy/hardener conductive agent was applied to the soldering points of the transducers and the high-temperature connecting terminals. Two thin layers of adhesive films were then placed in their designated positions for pre-bonding, followed by the placement of a PZT transducer on each layer. Blue tapes were used to secure the PZT transducers in place. Simultaneously, the high-temperature connecting terminals were positioned at the end of each printed circuit. Next, the Kapton[®] films, along with the connected PZT transducers and high-temperature connecting terminals, were subjected to a pre-curing process in an oven at 80 °C for 20 min. This pre-curing step aimed to prevent the conductive agents from flowing and causing short circuits during the subsequent vacuum and heating steps of the pre-bonding procedure.

After pre-curing, the Kapton[®] films with the embedded PZT transducers were placed on a vacuum-heated table. A vacuum was applied, and the assembly was heated to 150 °C for 1 h to initiate the bonding process. The vacuum was maintained throughout the cooling process until the assembly reached room temperature. Once the pre-bonding was completed, the blue tapes used to secure the PZT transducers were removed from each transducer. This process of applying conductive agents, pre-bonding the PZT transducers with adhesive films, and performing vacuum bonding at elevated temperature ensured secure and reliable connections between the PZT transducers and the high-temperature connecting terminals. The removal of the blue tapes after the pre-bonding step allowed for further processing and testing of the embedded PZT transducers in subsequent experiments.

The composite lay-up procedure when the Kapton preparation procedures were finished can be referred to in Figures 2 and 3. During the embedding, the resin films and prepared Kapton films with pre-bonded PZT transducers were placed in designated positions, as is shown in Figure 1b. The details of the whole embedding procedure can be referred to in the author's previous work [33]. When the fabrication was finished, two layers of adhesive films were placed between high-temperature connecting terminals and the surface of the composite laminates at the cut-out positions, and the release films were covered on top of these connecting terminals and fixed by blue tapes to prevent the resin from covering the surface of the connecting terminals.

After the curing process, the composite panels were inspected using a handheld DolphiCam ultrasonic camera to assess the quality of the embedded PZT transducers.

Following the inspection, the edges of the composite panels were trimmed. Connectors (RS 514–4408) were then mounted on the designated edges and bonded using superglue (RS 473–445). Finally, soldering was employed to establish the connection between the circuits and connectors. Figure 4 illustrates an example of a composite panel with embedded PZT transducers after the trimming process. The panel depicted in the figure has a thickness of 2 mm. The introduction of the cut-out method allowed for the precise trimming of composite edges while preserving the integrity of the embedded circuits. This approach facilitated the subsequent mounting of connectors and the establishment of reliable connections through soldering. The resulting composite panel with embedded PZT transducers exhibited a streamlined and functional design, as demonstrated in Figure 4.



Figure 4. Photo of the panel with embedded PZT transducers after trimming.

3. Ultrasonic Guided Waves (UGWs)

In this section, active sensing techniques were employed to investigate the response of ultrasonic guided waves (UGWs) in terms of in-plane motion. The focus was on studying the thickness effect on UGWs actuated and recorded by the embedded PZT transducers, with a comparison to previous results obtained from surface-mounted transducers. The aim was to analyze the amplitude and group velocity of the embedded UGWs and understand the influence of thickness on these parameters. This analysis is crucial for developing optimum excitation parameters for damage detection purposes in various plate thicknesses using embedded PZT transducers. The results obtained from active sensing were further utilized for damage detection and localization in structural health monitoring (SHM) applications.

To generate the actuation signal, a National Instrument (NI) PXI-5412 arbitrary signal generator was used, while a NI PXI-5105 digitizer was employed to record the measured UGW signals. The actuation signals utilized were five-cycle Hanning-windowed toneburst signals [37] with an input amplitude of 6 V. The sampling frequency was set to 100 MHz, with actuation frequencies of 50 kHz and 250 kHz for different experiments. Path 1–2 of the embedded PZT transducer pair, as shown in Figure 1a, was chosen for all three panels.

Figure 5a,b presents the extracted features of the peak amplitude and group velocity, respectively, for the first wave packet of embedded UGWs at 50 kHz and 250 kHz. The corresponding surface-mounted results are also included for comparison in Figure 5c,d. The peak amplitude was determined by selecting the peak of the envelope signals, while the group velocity was calculated by dividing the distance of the embedded PZT transducer pair path 1–2 by the time-of-arrival of the envelope signals. From Figure 5a, it can be observed that the peak amplitudes of both the A_0 and S_0 modes decrease with increasing thickness. In Figure 5b, it is evident that the group velocity of the A_0 mode decreases with increasing thickness at 50 kHz. On the other hand, the group velocity of the S_0 mode for the 9 mm thick panel is faster than that of the 2 mm thick panel but slower than that of the 4 mm thick panel at 250 kHz.

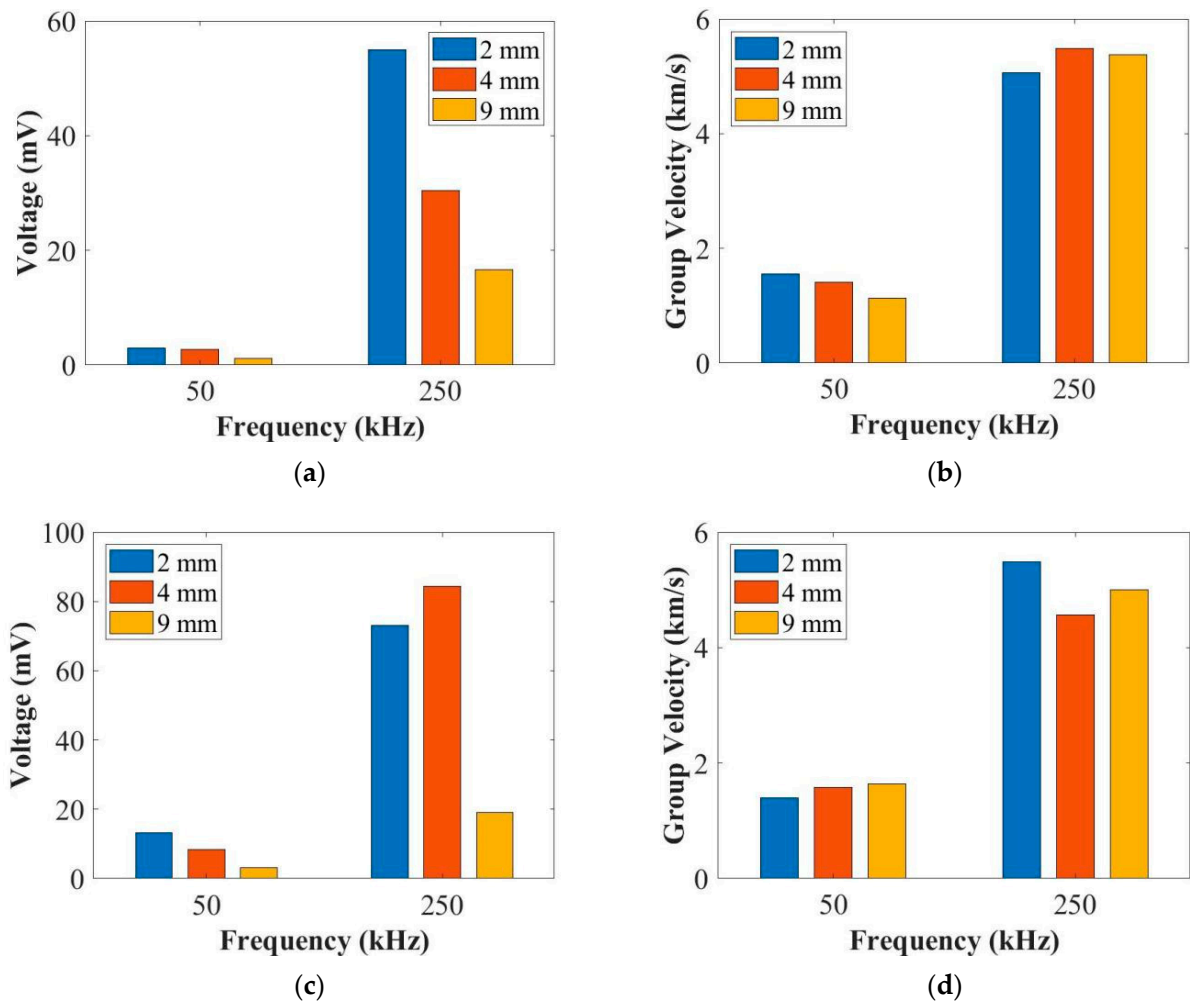


Figure 5. The summary of (a) the amplitude and (b) the group velocity of the embedded UGW and (c) the amplitude and (d) the group velocity of the surface-mounted UGW for the thickness of 2 mm, 4 mm, and 9 mm panels at 50 kHz and 250 kHz.

In summary, the thickness of the plate has an impact on the amplitudes of both the A_0 and S_0 modes of embedded UGWs. Additionally, the group velocity of the A_0 mode is influenced by the thickness, whereas the group velocity of the S_0 mode does not exhibit a significant dependence on thickness. These findings provide valuable insights into the behavior of UGWs and the influence of thickness when utilizing embedded PZT transducers. They contribute to the understanding of how to optimize excitation parameters for damage detection and localization in composite structures with different thicknesses, thereby enhancing the effectiveness of SHM applications.

Comparing the results obtained from embedded PZT transducers in Figure 5a,b with the surface-mounted PZT transducers in Figure 5c,d [21], some notable differences can be observed. In particular, the amplitude of the S_0 mode for the embedded signals exhibited a dependence on thickness at 250 kHz, whereas the amplitude of the surface-mounted signals did not show a similar trend. Additionally, the group velocity of the A_0 mode showed contrasting behaviors between the embedded and surface-mounted signals at 50 kHz. The group velocity decreased for the embedded signals as the thickness increased, while it increased for the surface-mounted signals. The reason behind these opposite relationships in the group velocity between the embedded and surface-mounted UGWs lies in the different bonding materials used. The embedded PZT transducers were bonded using resin films to comply with composite manufacturing specifications. On the other hand,

the surface-mounted PZT transducers were bonded using adhesive films. These different bonding materials give rise to variations in the propagation properties of the UGWs.

The bonding materials used in the embedding process, such as resin films, can introduce additional mechanical and acoustic coupling effects between the PZT transducers and the composite structure. These effects influence the UGW propagation and result in variations in the measured group velocity. In contrast, the adhesive films used for surface-mounted transducers may have different mechanical and acoustic properties, leading to distinct propagation characteristics and different relationships between group velocity and thickness. These findings highlight the significance of the bonding materials when comparing the results of embedded and surface-mounted PZT transducers. The choice of bonding material in SHM applications should be carefully considered to ensure accurate interpretation and reliable monitoring of UGW propagation characteristics in composite structures.

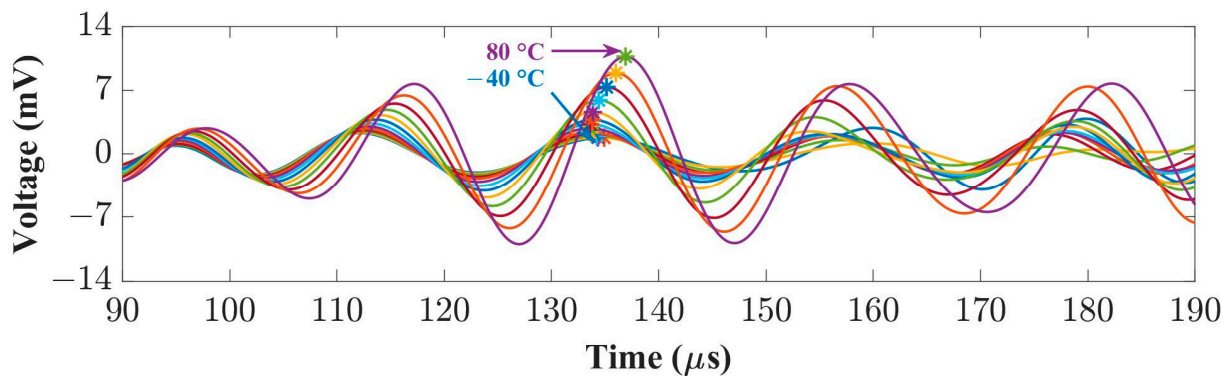
4. Temperature Influences on UGWs

Temperature changes can have a significant impact on the amplitude and phase of ultrasonic guided waves (UGWs), which can compromise the reliability of diagnosis if not properly compensated for. While several studies have investigated the influence of temperature on UGW signals in thick composite laminates [21,33,38], none of the research has reported whether the thickness of the composite laminate affects temperature compensation algorithms when using embedded PZT transducers. Therefore, in this section, the temperature influences on the peak amplitude and time-of-flight of the first wave packet of embedded signals were evaluated for panel thicknesses of 2 mm, 4 mm, and 9 mm.

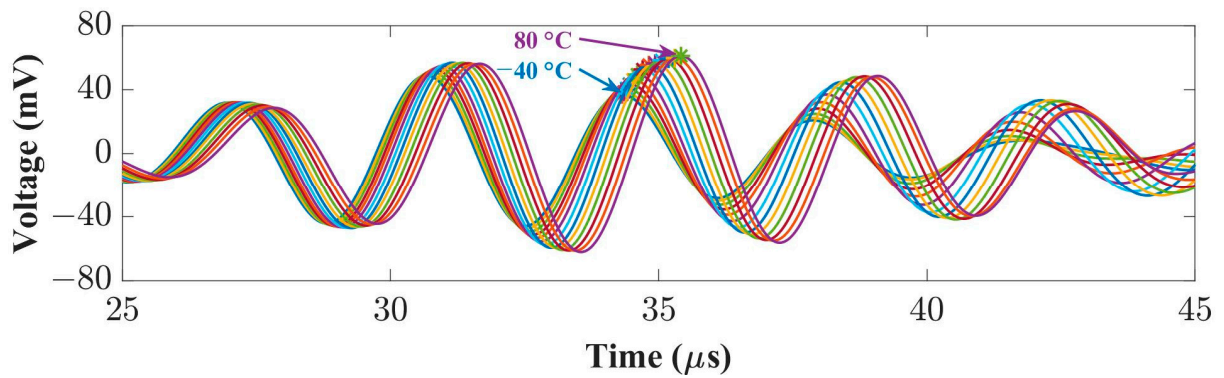
To assess the temperature effects, the composite panels were placed inside an environmental chamber, and the temperature range was set from $-40\text{ }^{\circ}\text{C}$ to $80\text{ }^{\circ}\text{C}$ with a temperature step of $10\text{ }^{\circ}\text{C}$. A transducer pair path 1–2, as shown in Figure 1a, was used for measurement. Five-cycle Hanning-windowed toneburst signals were employed at frequencies of 50 kHz and 250 kHz. Each composite panel was allowed to dwell at each temperature step for 20–30 min to ensure it reached the target temperature and maintained a stable state.

Figure 6 presents an example of the embedded signals at 50 kHz and 250 kHz for a 2 mm thick panel under different temperatures. The peak amplitude of each first wave packet of the embedded signals was automatically computed to measure amplitude reduction and phase shift. The analysis of the peak amplitude and time-of-flight of the embedded signals under varying temperatures provides insights into the temperature effects on UGW propagation and helps determine appropriate compensation algorithms. By quantifying the amplitude reduction and phase shift, the researchers can develop temperature compensation techniques that ensure accurate and reliable diagnosis in the presence of temperature variations.

Figures 7 and 8 present the relationships between temperature and the peak amplitude, as well as the time-of-flight (ToF) of the first wave packet of the embedded signals at 50 kHz (A_0 mode) and 250 kHz (S_0 mode) for the 2 mm, 4 mm, and 9 mm thick panels. These figures also include the surface-mounted results for comparison. In Figure 7a, the peak amplitude of the A_0 mode exhibits an increasing trend with temperature for all panel thicknesses at 50 kHz. However, the slopes of the amplitude increase vary for different thicknesses. Similarly, in Figure 7b, the peak amplitude of the S_0 mode shows temperature dependence at 250 kHz. For the 2 mm and 9 mm thick panels, the amplitude increases with temperature, while for the 4 mm thick panel, the amplitude decreases as temperature increases.

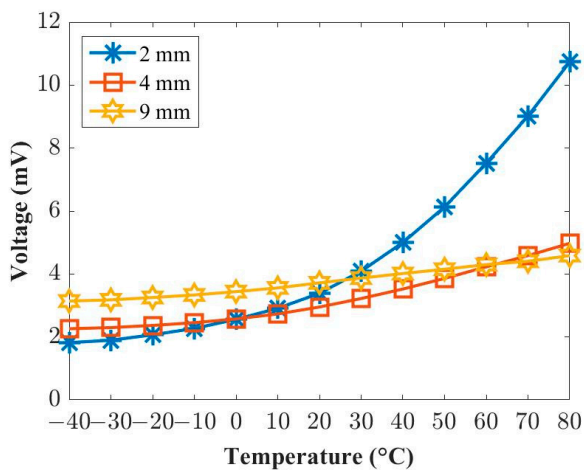


(a)

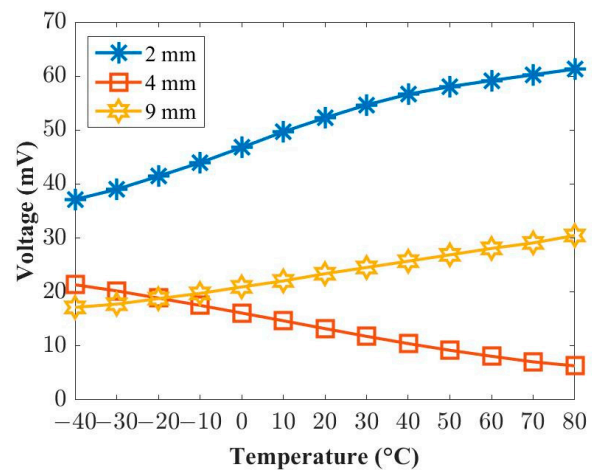


(b)

Figure 6. Examples of embedded UGWs under different temperatures at (a) 50 kHz and (b) 250 kHz.

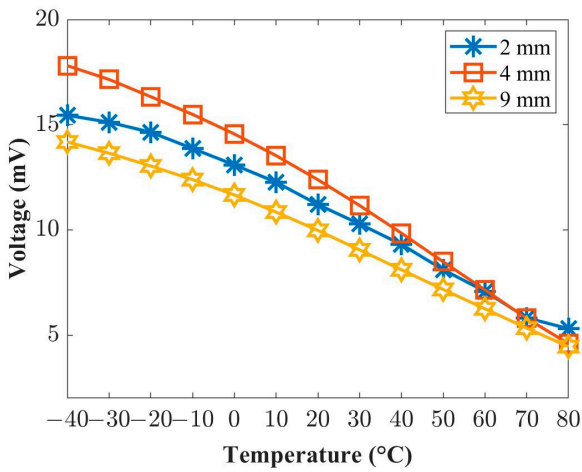


(a)

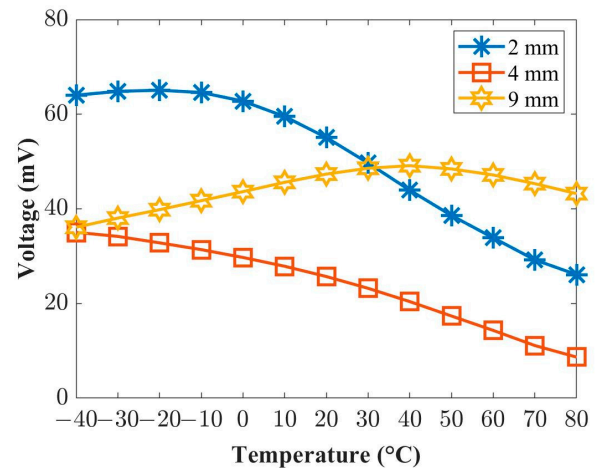


(b)

Figure 7. Cont.

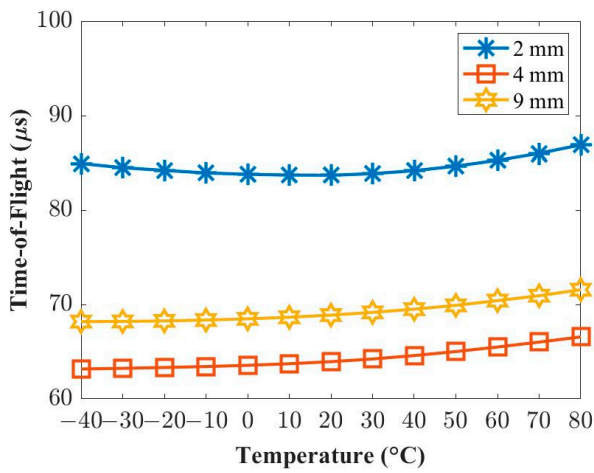


(c)

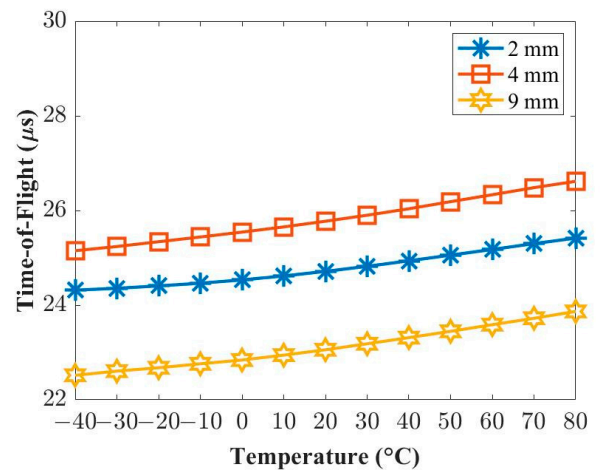


(d)

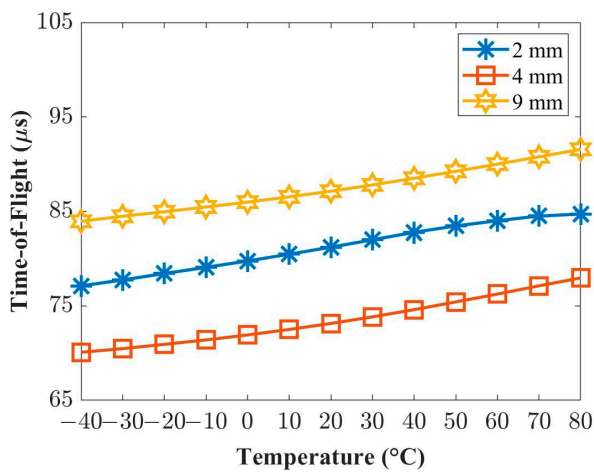
Figure 7. Relationships of the temperature with the peak amplitude at (a) 50 kHz and (b) 250 kHz for embedded UGW and at (c) 50 kHz and (d) 250 kHz for surface-mounted UGW.



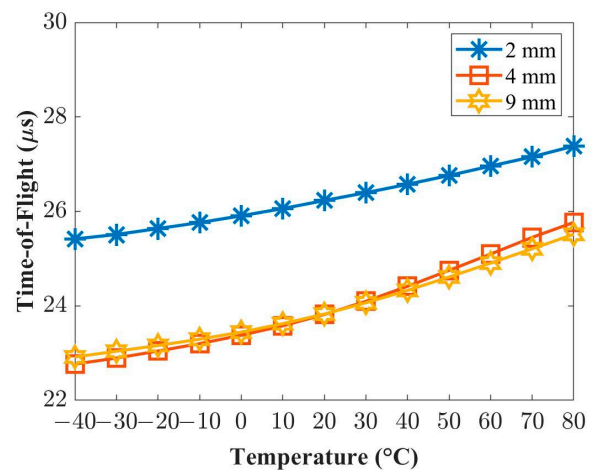
(a)



(b)



(c)



(d)

Figure 8. Relationships of the temperature with the time-of-flight at (a) 50 kHz and (b) 250 kHz for embedded UGW and at (c) 50 kHz and (d) 250 kHz for surface-mounted UGW.

Figure 8a illustrates the ToF of the A_0 mode for the 2 mm thick panel. It initially decreases from $-40\text{ }^\circ\text{C}$ to $20\text{ }^\circ\text{C}$ and then increases from $20\text{ }^\circ\text{C}$ to $80\text{ }^\circ\text{C}$ at 50 kHz. However, for the 4 mm and 9 mm thick panels, the ToF increases with temperature. In Figure 8b, the ToF of the S_0 mode increases with temperature for all panel thicknesses at 250 kHz. These findings highlight the temperature effects on the peak amplitude and ToF of the embedded signals for different thicknesses. The amplitude and ToF variations with temperature provide insights into the behavior of UGWs and the need for temperature compensation algorithms. Understanding these relationships is crucial for developing accurate and reliable SHM systems that account for temperature variations in composite structures. The comparisons with the surface-mounted results help to identify the influence of embedding on the temperature response of the UGW signals.

In conclusion, the temperature had a significant impact on the peak amplitude and time-of-flight (ToF) of the first wave packet in UGW signals for panel thicknesses of 2 mm, 4 mm, and 9 mm. The peak amplitudes of the A_0 and S_0 modes generally increased with temperature, except for the S_0 mode of the 4 mm thick panel at 250 kHz. The ToF increased with temperature, except for the 2 mm thick panel at 50 kHz.

Comparing the embedded temperature results to the surface-mounted temperature results in Figure 7c,d, some differences can be observed. For the peak amplitude of the A_0 mode (50 kHz), it decreased for the surface-mounted signals but increased for the embedded signals with increasing temperature for all panel thicknesses. Similarly, for the peak amplitude of the S_0 mode (250 kHz), the surface-mounted signals initially increased and then decreased with temperature, while the embedded signals consistently increased, but only for the 2 mm thick panel. Additionally, the ToF of the A_0 mode (50 kHz) increased for the surface-mounted signals but showed a decrease followed by an increase for the embedded signals in the 2 mm thick panel.

These differences in temperature responses between embedded and surface-mounted signals highlight the influence of embedding on the behavior of UGWs. The bonding materials and coupling mechanisms in the embedding process can lead to variations in the temperature sensitivity of the UGW signals. Understanding these differences is crucial for developing accurate temperature compensation algorithms in SHM applications, especially when using embedded PZT transducers. Thermal expansions, for example, can have an impact on the relationship between peak amplitude, time-of-flight (ToF), and temperature. Changes in composite properties, such as density and thickness, as well as the dimensions of the PZT transducers and the propagation distances of UGWs, are influenced by thermal expansions. These changes, in turn, can affect the dispersion properties of composites, which are associated with the group velocity of UGWs and the thickness of the composite panel. Consequently, the difference in ToF at 50 kHz for the 2 mm thick panel compared to the other thicker panels may be due to the thickness-dependent dispersion properties of composites.

Another factor to consider is the piezoelectric constants (d_{31} and g_{31}), which can affect the mechanical properties and piezo sensitivity between the embedded and surface-mounted PZT transducers. These properties have an impact on the amplitude properties of UGWs. Therefore, it is important to establish the relationship between phase and amplitude changes for composite panels, particularly in relation to their thickness, to develop reliable compensation algorithms for damage detection under different temperatures.

Additionally, the PZT transducers and their bonding properties can be influenced by temperature-induced changes. The use of resin films for the embedded panels during the lay-up, as opposed to adhesive films for the panels with surface-mounted PZT transducers, can lead to differences in the temperature response. The selection of bonding materials, such as the resin film and adhesive film, is another factor that can affect the temperature results and should be carefully considered.

Taking these factors into account ensures a comprehensive understanding of the temperature effects on UGWs and allows for the development of accurate compensation algorithms and reliable damage detection in composite structures under varying temperature conditions.

5. Damage Detection and Localization

Here, the focus is on differentiating the interaction of ultrasonic guided waves (UGWs) with surface artificial damage and impact damage, specifically interlaminar delamination and debonding, in composite panels with varying thicknesses. The configurations of PZT transducers for damage detection and localization are shown in Figure 1. To simulate surface artificial damage, an added mass in the form of weighted Blu Tack was applied to the surface of the panels. This allowed for reusability of the panels before conducting the impact tests. The impact tests were then performed to create barely visible impact damage in the composite panels. These impact events resulted in interlaminar delamination and debonding, which are common types of damage observed in composite structures.

For damage detection, two methods were employed: the correlation coefficient and the delay-and-sum (DAS) algorithm. The correlation coefficient measures the similarity between the baseline (undamaged) UGW signals and the current UGW signals, providing a measure of the damage index. The theory and calculation of the damage index using the correlation coefficient can be referred to [22]. The DAS algorithm, on the other hand, utilizes the differences between the baseline and current UGW signals to detect and locate the damage. The theory and implementation of the DAS algorithm for damage detection can be found in the references [39,40]. By employing these damage detection techniques, the researchers aim to demonstrate the effectiveness of distinguishing between surface artificial damage and impact damage using UGWs. The comparison of results for panels with different thicknesses provides insights into the influence of thickness on the detection and localization of various types of damage in composite structures.

5.1. Surface-Mounted Artificial Damage

Figure 9 illustrates the placement of the weighted Blu Tack, which simulates surface-mounted artificial damage, on the surface of the 2 mm thick panel. The weighted Blu Tack is positioned in a designated location, typically off-center, to mimic the presence of localized damage on the composite surface. This configuration allows for the investigation of damage detection and localization using the correlation coefficient and the delay-and-sum (DAS) algorithm for panels with different thicknesses, including 2 mm, 4 mm, and 9 mm.



Figure 9. Photo of a weighted Blu Tack placed on the surface of the 2 mm thick panel.

The correlation coefficient and the DAS algorithm are applied to analyze the differences between the baseline (undamaged) UGW signals and the current UGW signals obtained from the damaged panels. These techniques enable the detection and localization of surface-mounted artificial damage, providing insights into the effectiveness of the damage detection methods across different panel thicknesses. By studying the results obtained from the correlation coefficient and the DAS algorithm, the researchers can evaluate the impact of panel thickness on the accuracy and reliability of damage detection and localization for surface-mounted artificial damage. This analysis contributes to a comprehensive

understanding of the thickness effects on the performance of structural health monitoring techniques in composite structures.

Figures 10–15 present the results of damage detections and localizations for the panel thicknesses of 2 mm, 4 mm, and 9 mm at 50 kHz and 250 kHz, respectively. These figures also include the surface-mounted results for comparison. For the 4 mm panel, it is important to note that the embedded circuits of PZT transducer 1 shown in Figure 1 became disconnected during the manufacturing process. As a result, only three embedded PZT transducers were available for damage detection and localizations in this panel. Regarding the 9 mm panel, the much higher amplitude of crosstalk introduced interference in the first wave packet of the measured signal for pair paths 1–3/3–1 and 2–4/4–2 shown in Figure 1 at 50 kHz. This interference made it difficult to accurately identify the time-of-arrival of the measured signals for the aforementioned pair paths. Consequently, the correlation coefficient and DAS algorithm based on the time-of-arrival information could not be effectively used for damage detection and localization at 50 kHz.

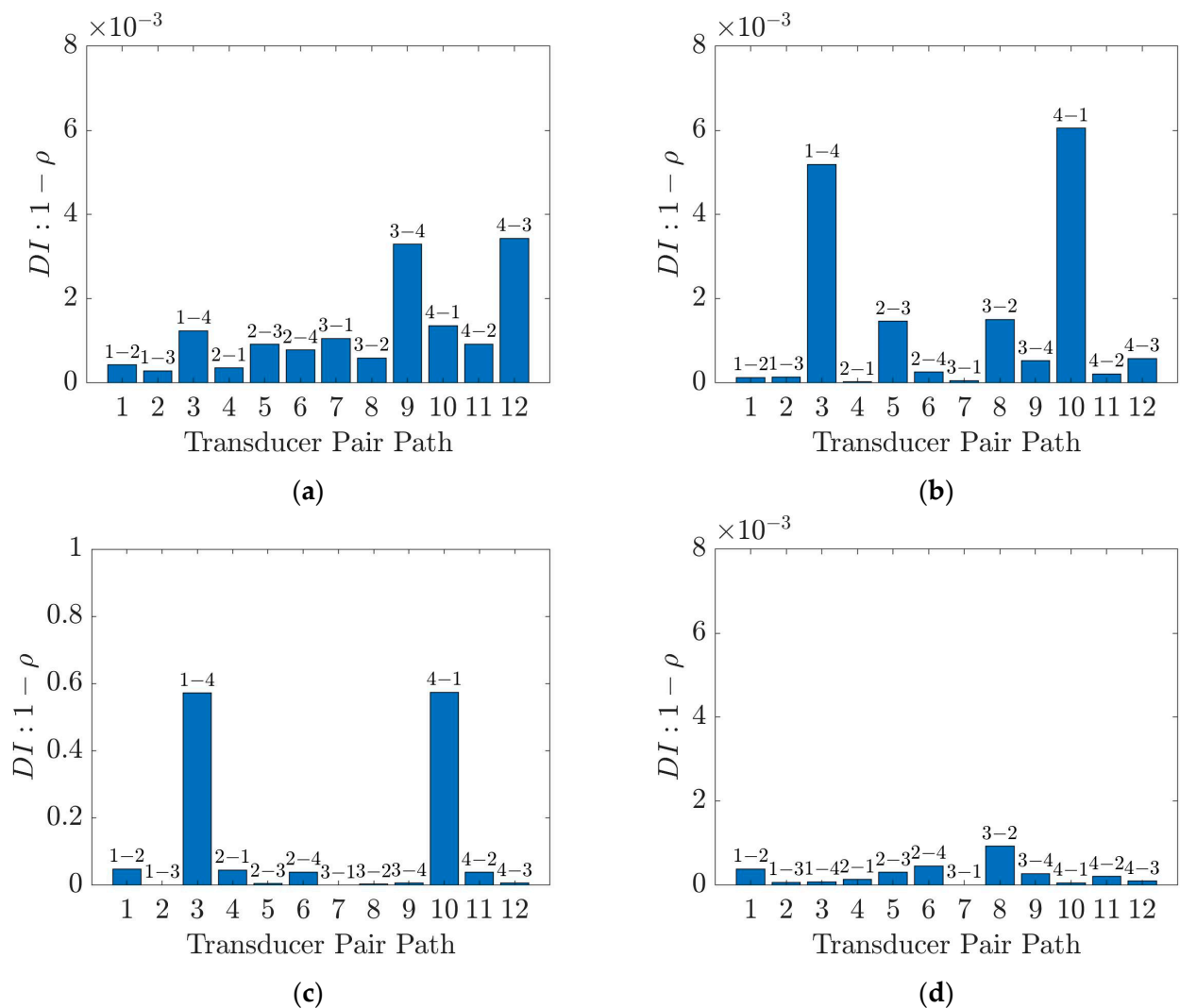


Figure 10. Detections of surface-mounted artificial damage for the 2 mm thick panel at (a) 50 kHz and (b) 250 kHz using embedded PZT transducers and at (c) 50 kHz and (d) 250 kHz using surface-mounted PZT transducers.

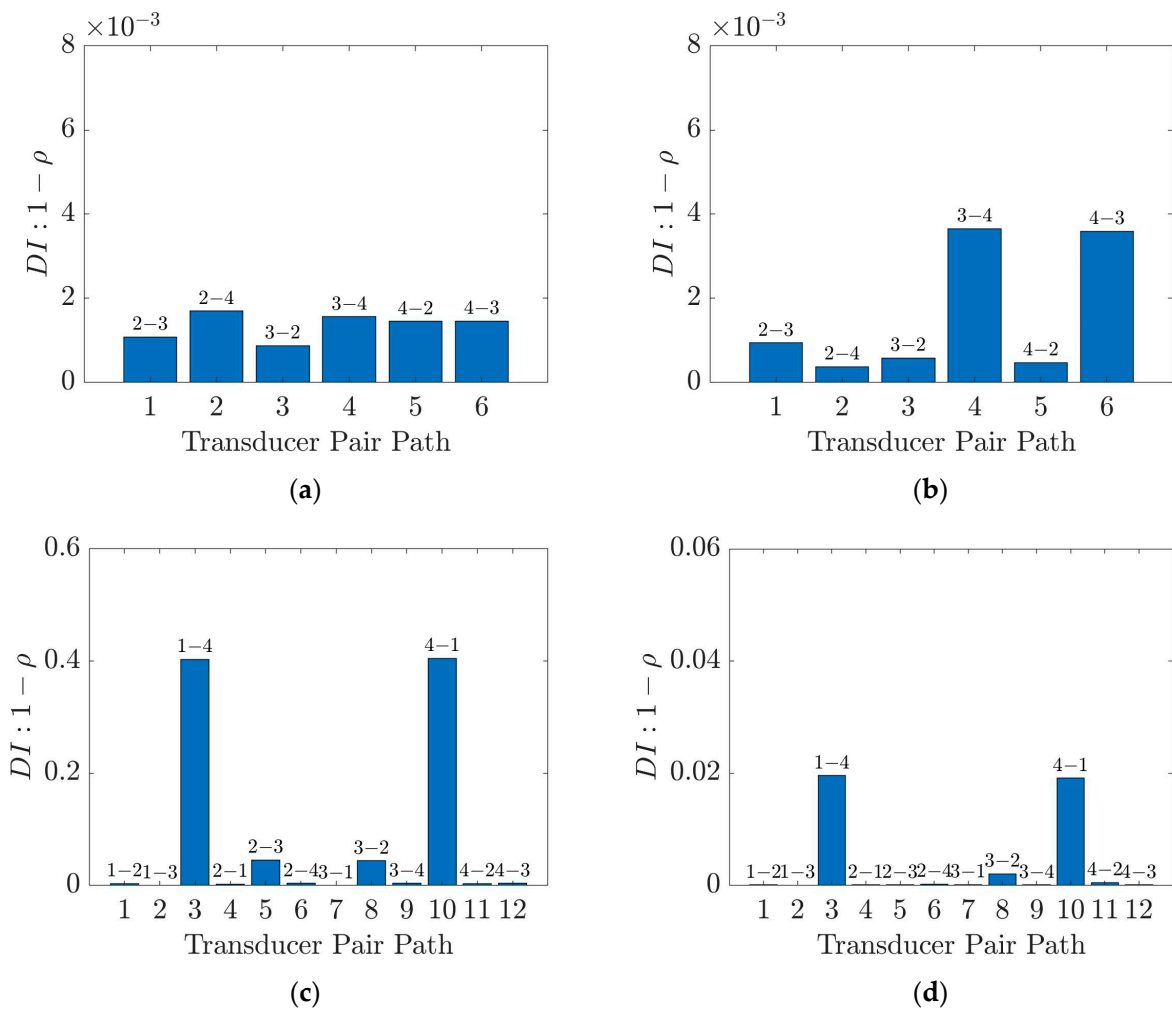


Figure 11. Detections of surface-mounted artificial damage for the 4 mm thick panel at (a) 50 kHz and (b) 250 kHz using embedded PZT transducers and at (c) 50 kHz and (d) 250 kHz using surface-mounted PZT transducers.

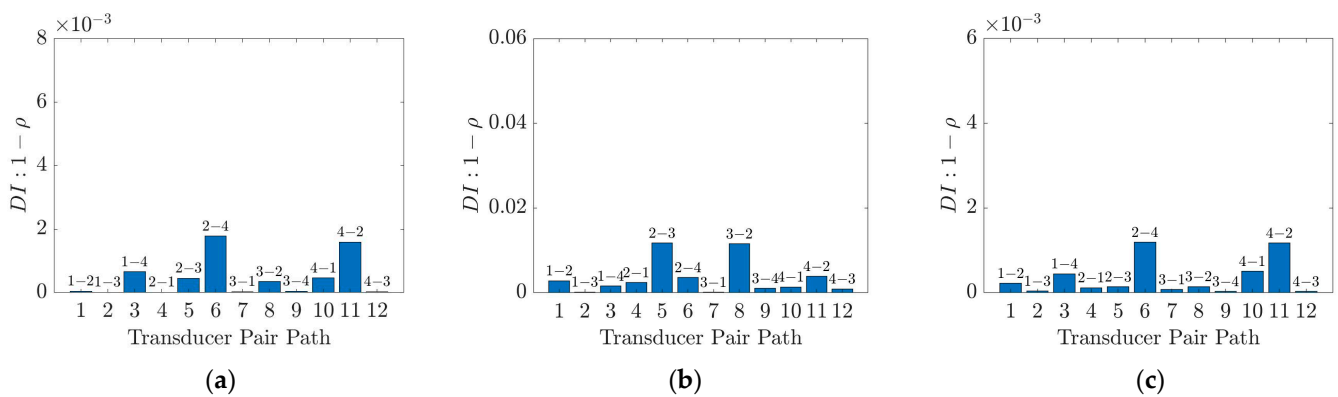


Figure 12. Detections of surface-mounted artificial damage for the 9 mm thick panel at (a) 250 kHz using embedded PZT transducers and at (b) 50 kHz and (c) 250 kHz using surface-mounted PZT transducers.

The presented results highlight the outcomes of the damage detection and localization process using the correlation coefficient and DAS algorithm for different panel thicknesses. The comparisons with the surface-mounted results offer insights into the performance differences between embedded and surface-mounted PZT transducers for damage detection and localization. By examining these results, the researchers can evaluate the efficacy and

limitations of the damage detection techniques across different panel thicknesses, contributing to the advancement of structural health monitoring methods for composite structures.

From the analysis of Figures 10–15, several conclusions can be drawn regarding the damage detection and localization results using embedded PZT transducers compared to surface-mounted PZT transducers:

The Damage Index (DI) values:

The DI values for the S_0 mode are generally higher than those for the A_0 mode, indicating that the S_0 mode is more suitable for surface-related damage detection. The DI values decrease with increased thickness at both 50 kHz and 250 kHz, indicating that the DI values of the S_0 and A_0 modes of embedded UGWs are thickness-dependent. Compared to surface-mounted results, the DI values for the A_0 mode of embedded UGWs are lower, while those for the S_0 mode of embedded UGWs are higher. This is because the A_0 mode is out-of-plane dominant, while the S_0 mode is in-plane dominant.

Damage localization:

The surface-mounted artificial damage can be accurately located using embedded PZT transducers, even for thick composite panels (e.g., 9 mm). The embedded PZT transducers demonstrate better sensitivity in locating surface-mounted artificial damage in thick composite laminates compared to surface-mounted PZT transducers, as shown in Figure 15. These findings highlight the advantages of using embedded PZT transducers for damage detection and localization in thick composite laminates. The embedded transducers exhibit higher sensitivity and accuracy in locating surface-mounted artificial damage compared to surface-mounted transducers. Additionally, the choice of the appropriate UGW mode (S_0 or A_0) depends on the nature of the damage and the specific requirements of the application.

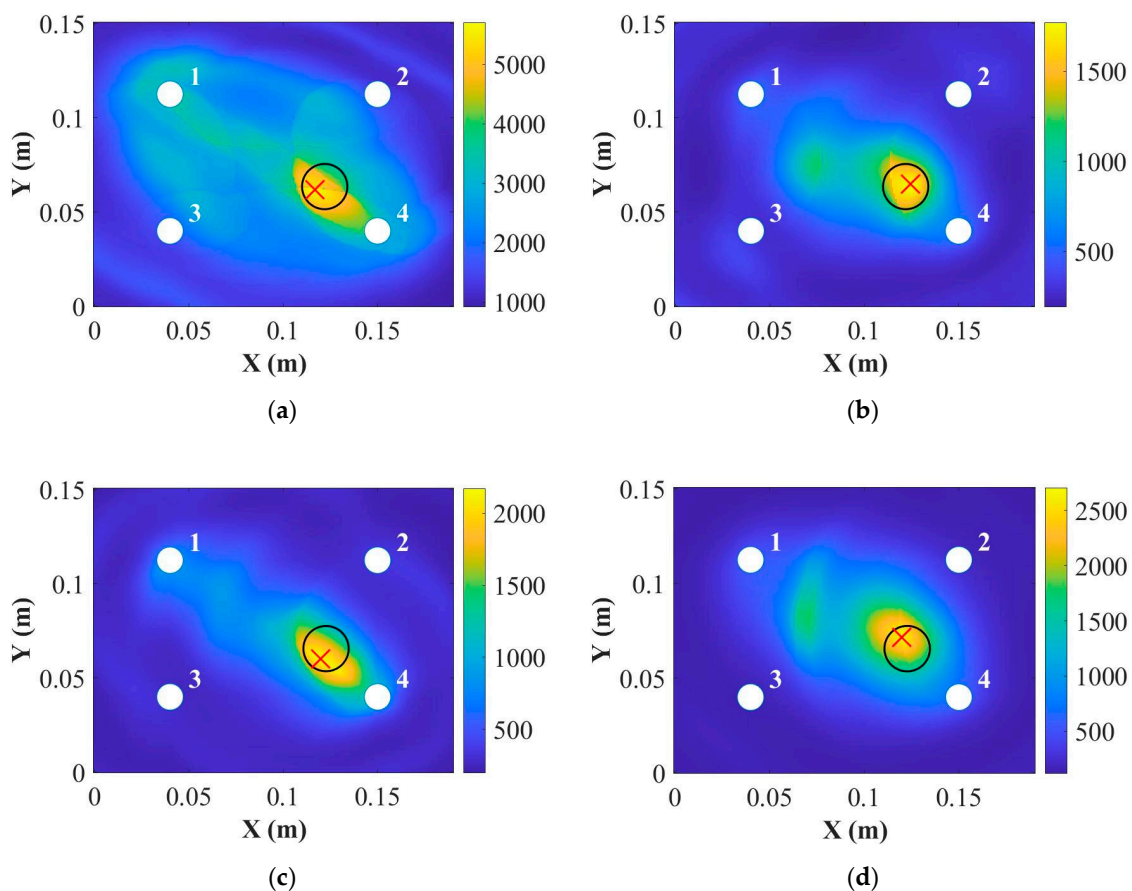


Figure 13. Localizations of surface-mounted artificial damage for the 2 mm thick panel at (a) 50 kHz and (b) 250 kHz using embedded PZT transducers and at (c) 50 kHz and (d) 250 kHz using surface-mounted PZT transducers (where the “○” is the position for real damage and the “×” is the position for predicted damage).

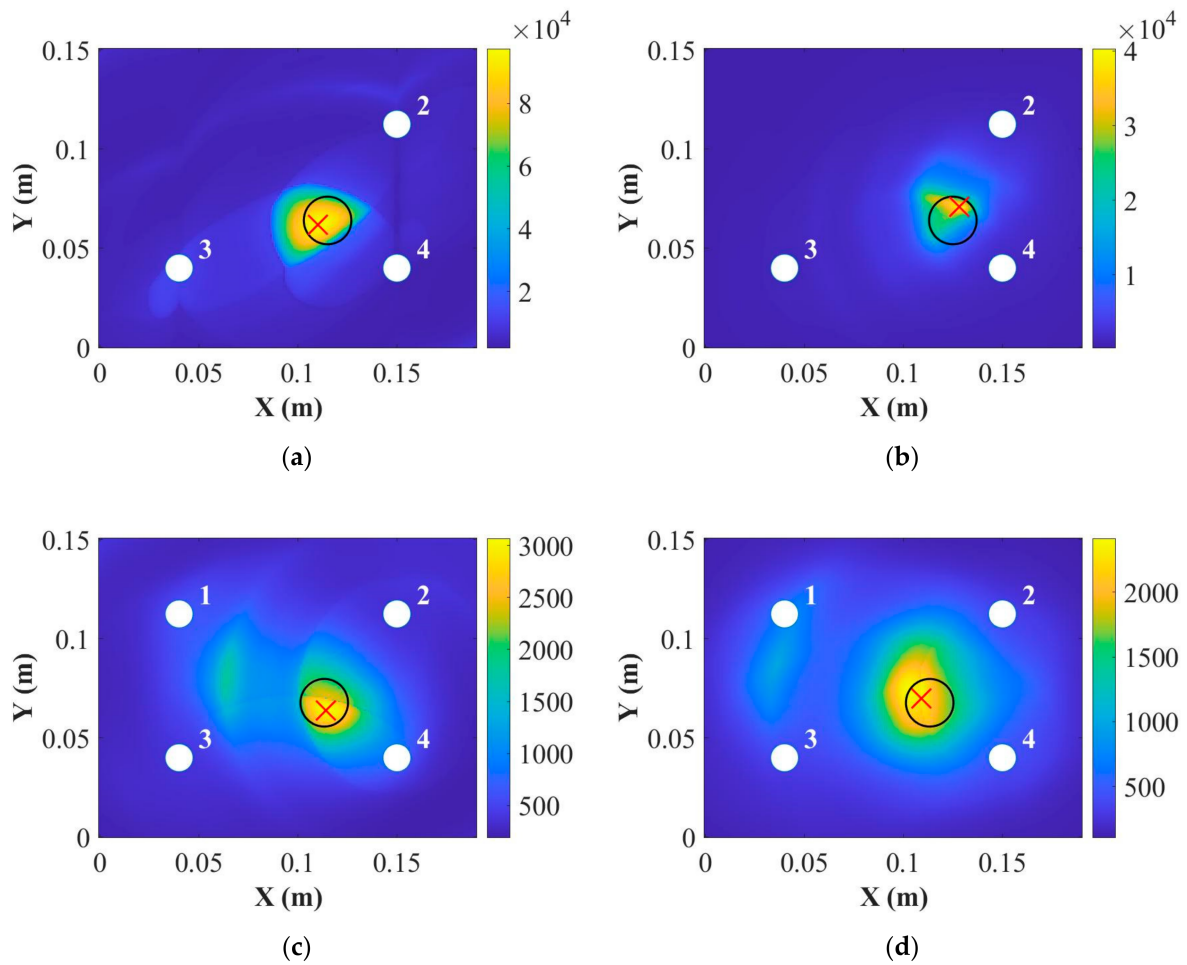


Figure 14. Localizations of surface-mounted artificial damage for the 4 mm thick panel at (a) 50 kHz and (b) 250 kHz using embedded PZT transducers and at (c) 50 kHz and (d) 250 kHz using surface-mounted PZT transducers (where the “○” is the position for real damage and the “×” is the position for predicted damage).

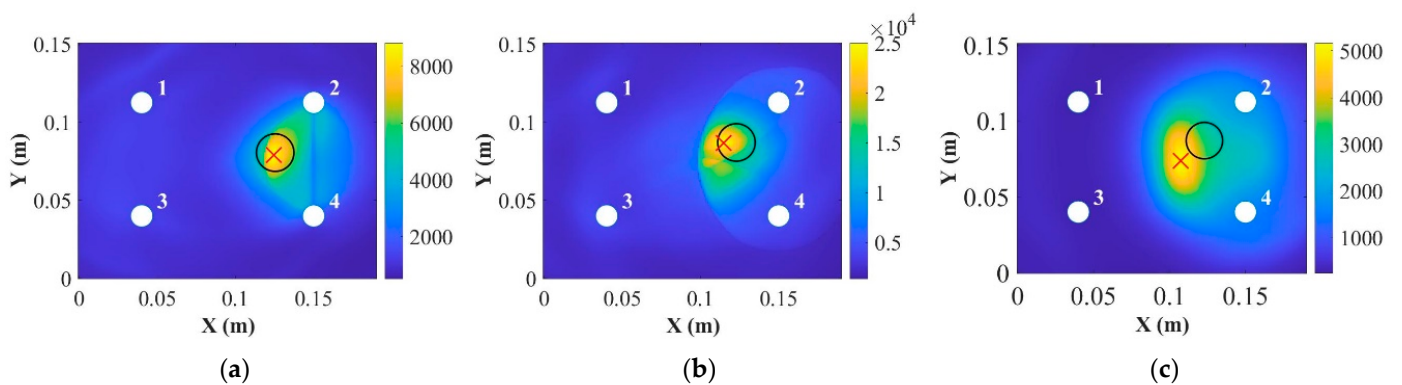


Figure 15. Localizations of surface-mounted artificial damage for the 9 mm thick panel at (a) 250 kHz using embedded PZT transducers and at (b) 50 kHz and (c) 250 kHz using surface-mounted PZT transducers (where the “○” is the position for real damage and the “×” is the position for predicted damage).

5.2. Impact Damage

To investigate the thickness effects on the detection of real barely visible impact damage (BVID) in composites using embedded ultrasonic guided waves (UGWs), impact tests were conducted on composite panels with thicknesses of 2 mm, 4 mm, and 9 mm.

The impact tests were performed using a drop tower, specifically the INSTRON CEAST 9350, as shown in Figure 16. The impact position for each panel was the same as that used for the surface-mounted artificial damage in Section 5.1. The impact energy was initially set at a relatively low level and increased incrementally by 2 J for each impact test. After each impact, the impact area was inspected using a DolphiCam C-scan (CF08) to identify the resulting damage. The impact energy was increased until a suitable damage area was detected and captured by the C-scan.

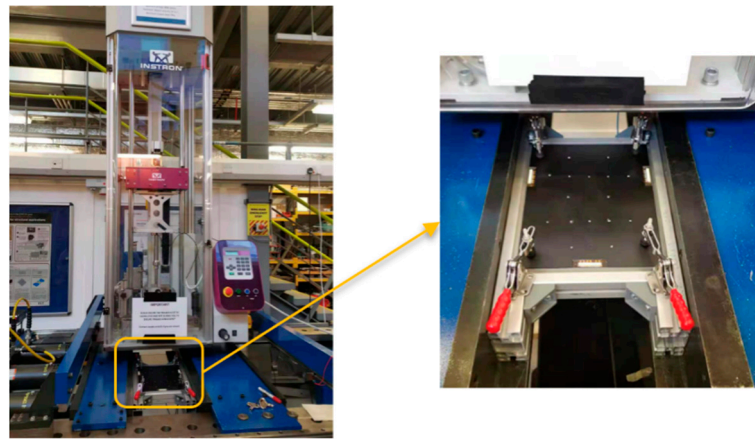


Figure 16. INSTRON CEAST 9350 drop tower for the impact test.

The impactor used in the tests was a hemisphere with a diameter of 20 mm. The load cell used for the 2 mm thick panel was a 22 kN load cell with an additional 3 kg mass, while a 90 kN load cell with the same additional mass was used for the 4 mm and 9 mm thick panels. The impact energy and velocity values used for each panel were as follows: 15 J and 3.53 m/s for the 2 mm thick panel, 20 J and 2.72 m/s for the 4 mm thick panel, and 57 J and 4.59 m/s for the 9 mm thick panel, respectively. These impact tests provide the basis for evaluating the detection and characterization of real BVID in composite panels of different thicknesses using embedded UGWs. The impact parameters were carefully chosen to achieve suitable damage areas for subsequent analysis and assessment.

Figure 17 illustrates the results of the non-destructive inspection (NDI) using the DolphiCam C-scan (CF08) for the impact damage on each composite panel. The following observations can be made based on the figure:

- (a) For the 2 mm thick panel (Figure 17a), the detected damage area was approximately 176 mm², and the damage thickness was measured to be around 1.2 mm from the impact surface. Additionally, surface cracks were visible on the panel after the impact test.
- (b) In the case of the 4 mm thick panel (Figure 17b), the detected damage area was approximately 452 mm². The horizontal and vertical B-scans indicated a damage thickness of approximately 3 mm from the impact surface. Similar to the 2 mm thick panel, surface cracks were also observed.
- (c) For the 9 mm thick panel (Figure 17c), the detected area of the impact damage was around 254 mm². The horizontal and vertical B-scans revealed a damage thickness of approximately 2 mm from the impact surface. Surface cracks were also visible on this panel following the impact test.

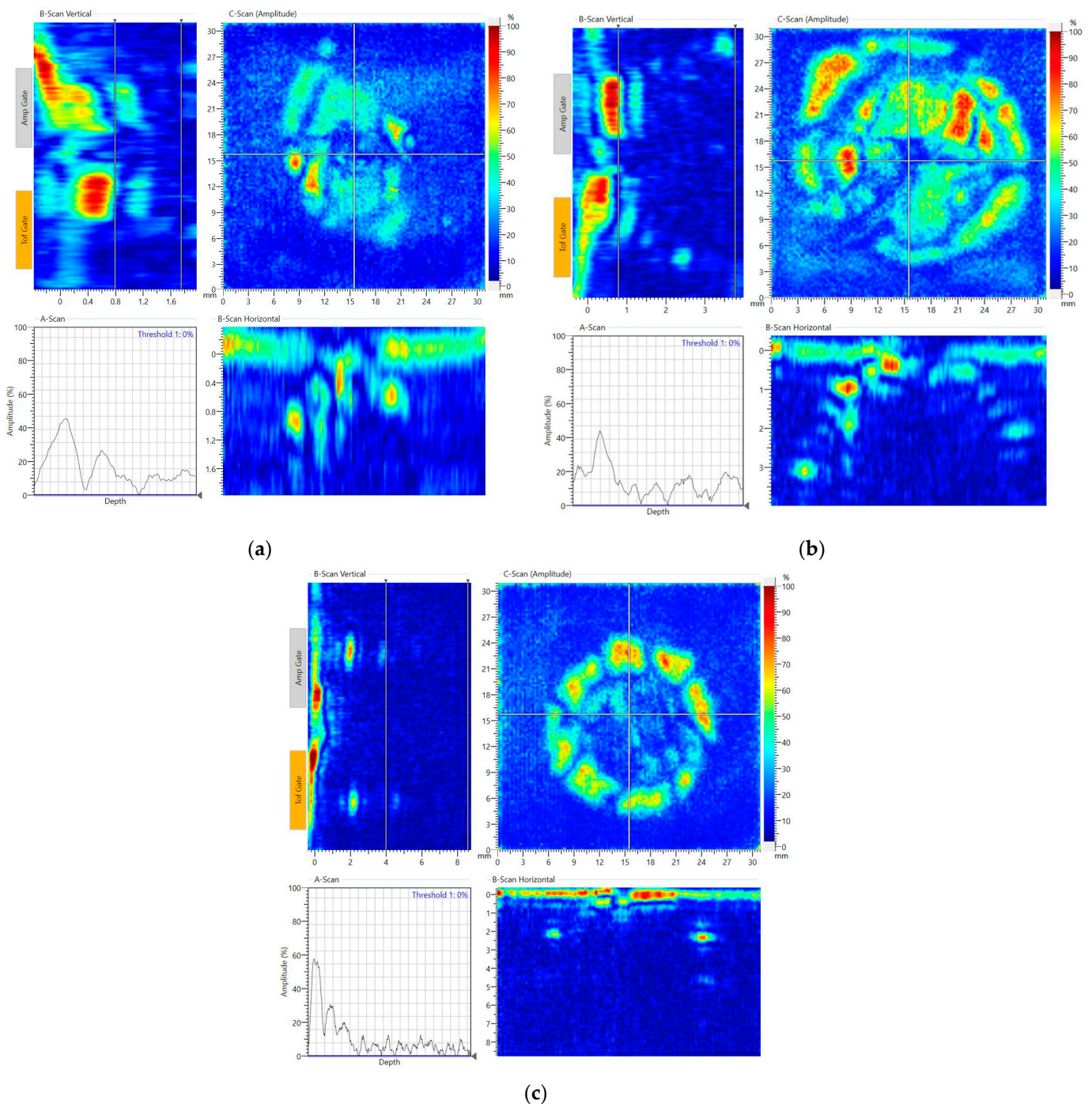


Figure 17. C-scan results of the impact damage at (a) 15 J for the 2 mm panel, (b) 20 J for the 4 mm panel, and (c) 57 J for the 9 mm panel.

These NDI results provide visual evidence of the impact damage inflicted on each composite panel. The DolphiCam C-scan successfully captured the extent and location of the damage, as well as the presence of surface cracks. These findings will serve as a basis for further analysis and comparison with the results obtained from the embedded UGW measurements for damage detection and localization.

In this section, the correlation coefficient and the delay-and-sum (DAS) algorithm were employed to detect and localize the impact damage for composite panels with thicknesses of 2 mm, 4 mm, and 9 mm. Figures 18–23 display the comparisons between the embedded and surface-mounted results for damage detection and localization at frequencies of 50 kHz

and 250 kHz, respectively. In Figures 18–20, the damage index (DI) values of embedded results for the A_0 and S_0 modes were lower than those of surface-mounted results for each thickness panels. However, it should be noted that the DI values will not be compared among the thickness of 2 mm, 4 mm, and 9 mm panels due to the different impact energies of each panel. In addition, the results also demonstrate that the damage index is capable of detecting the presence of impact damage for all three panel thicknesses.

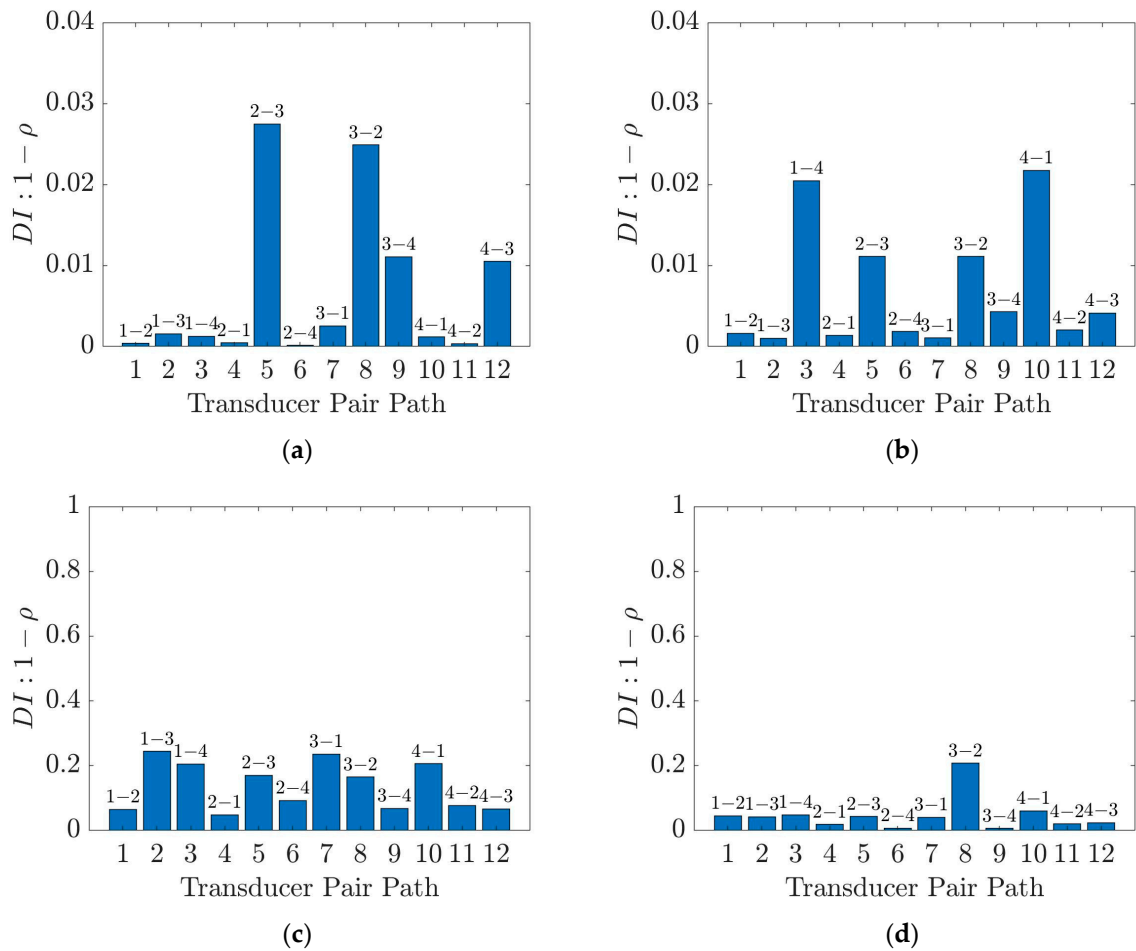


Figure 18. Detections of impact damage for the 2 mm thick panel at (a) 50 kHz and (b) 250 kHz using embedded PZT transducers and at (c) 50 kHz and (d) 250 kHz using surface-mounted PZT transducers.

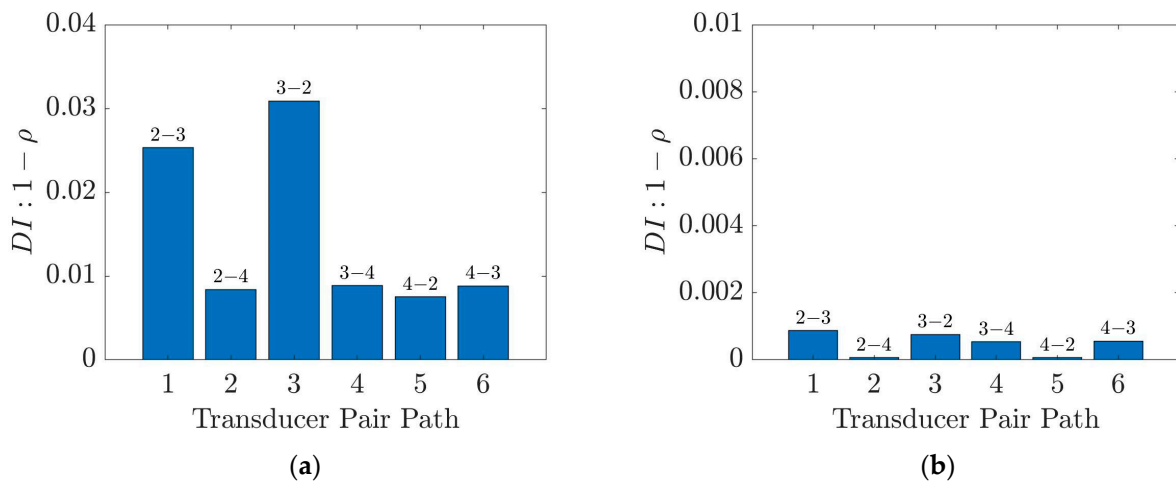


Figure 19. Cont.

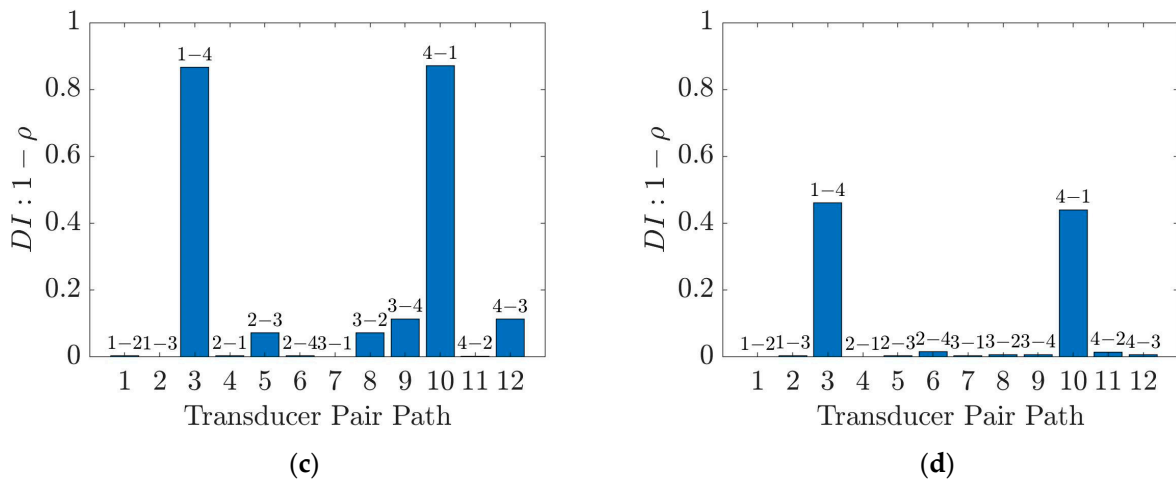


Figure 19. Detections of impact damage for the 4 mm thick panel at (a) 50 kHz and (b) 250 kHz using embedded PZT transducers and at (c) 50 kHz and (d) 250 kHz using surface-mounted PZT transducers.

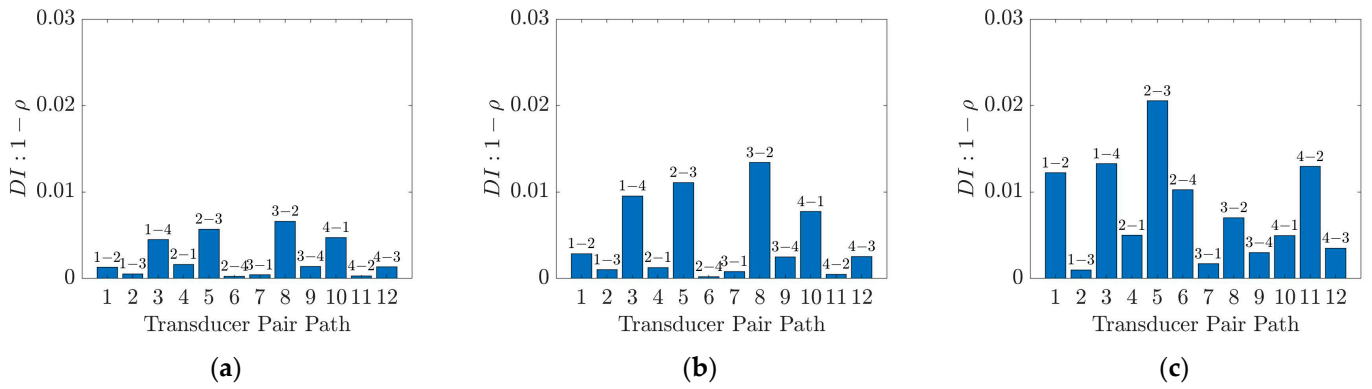


Figure 20. Detections of impact damage for the 9 mm thick panel at (a) 50 kHz using embedded PZT transducers and at (b) 50 kHz and (c) 250 kHz using surface-mounted PZT transducers.

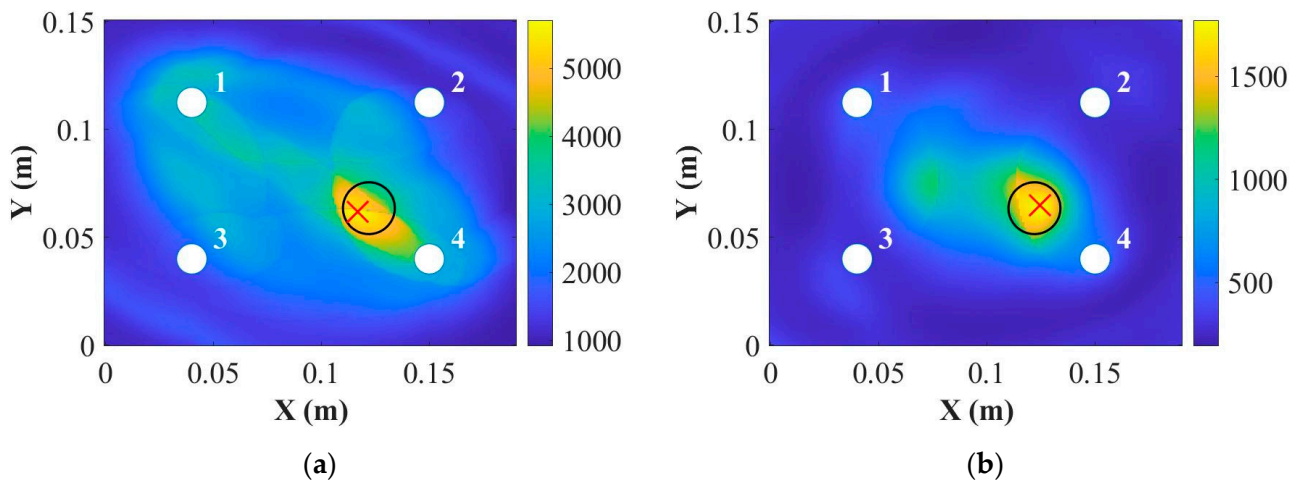


Figure 21. Cont.

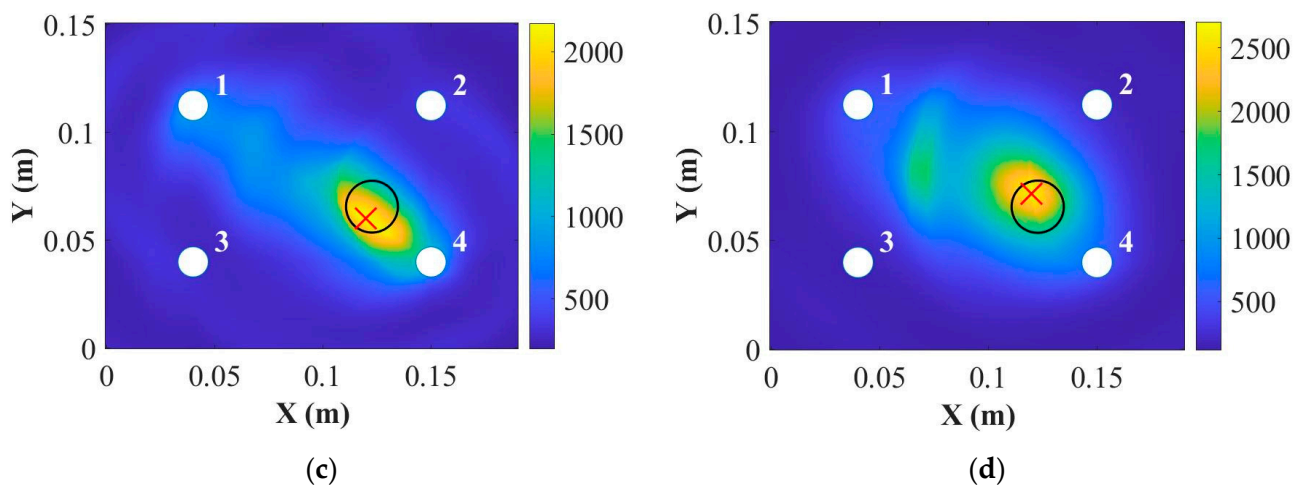


Figure 21. Localization of impact damage for the 2 mm thick panel at (a) 50 kHz and (b) 250 kHz using embedded PZT transducers and at (c) 50 kHz and (d) 250 kHz using surface-mounted PZT transducers (where the “○” is the position for real damage and the “×” is the position for predicted damage).

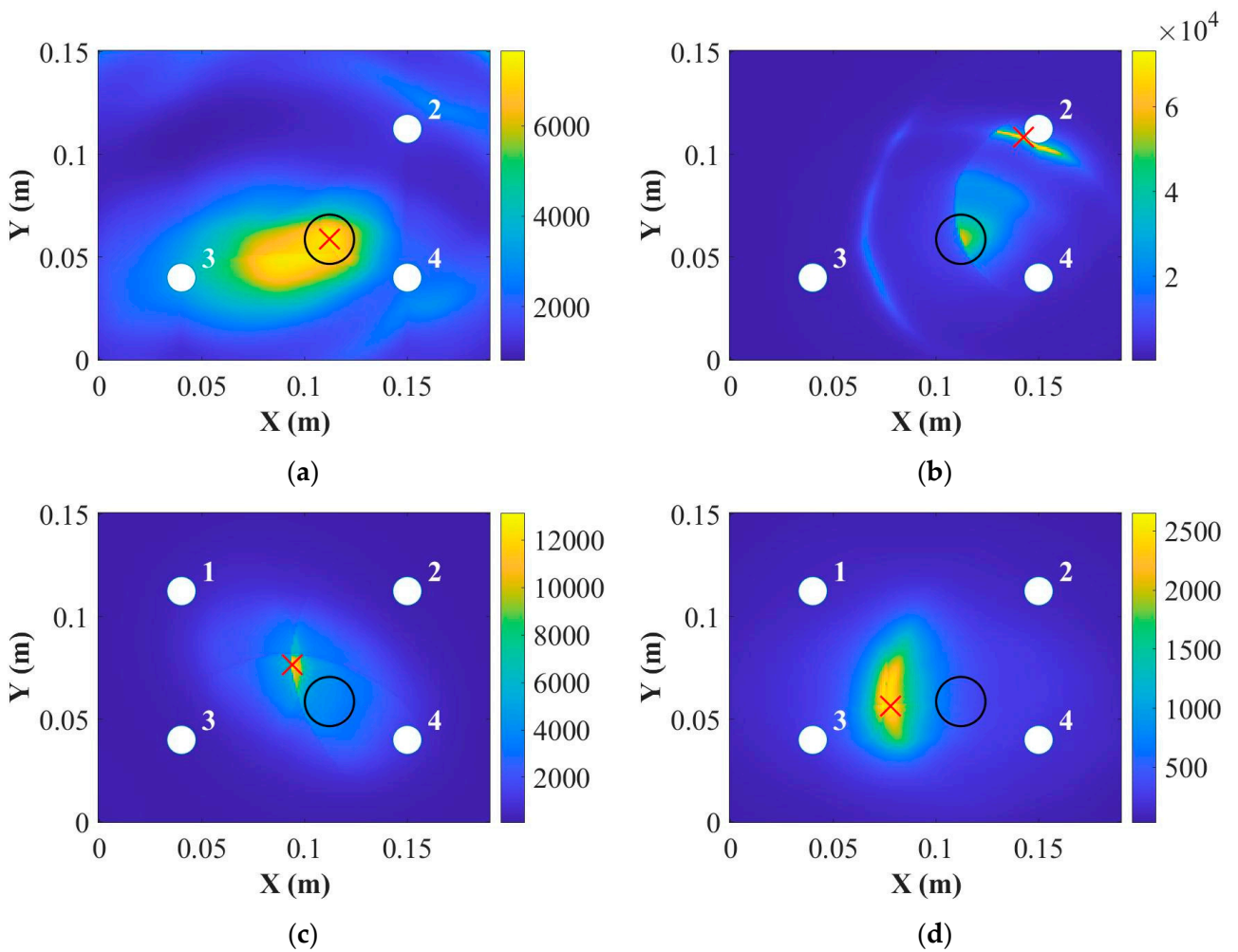


Figure 22. Localization of impact damage for the 4 mm thick panel at (a) 50 kHz and (b) 250 kHz using embedded PZT transducers and at (c) 50 kHz and (d) 250 kHz using surface-mounted PZT transducers (where the “○” is the position for real damage and the “×” is the position for predicted damage).

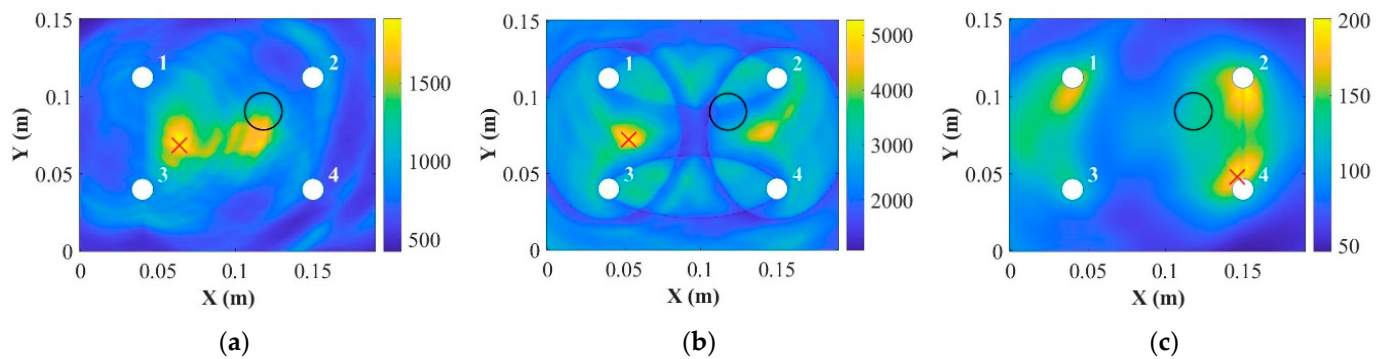


Figure 23. Localization of impact damage for the 9 mm thick panel at (a) 250 kHz using embedded PZT transducers and at (b) 50 kHz and (c) 250 kHz using surface-mounted PZT transducers (where the “○” is the position for real damage and the “×” is the position for predicted damage).

Additionally, in Figures 21–23, the DAS algorithm is effective in accurately locating the damage position for the 2 mm and 4 mm thick panels at 50 kHz. However, the DAS algorithm is unable to accurately locate the impact damage for all three panel thicknesses at 250 kHz. Overall, the findings indicate that the A_0 mode at 50 kHz is more suitable for accurately locating the impact damage. This conclusion is consistent with previous experimental results utilizing surface-mounted PZT transducers [28]. It is worth noting that the DAS algorithm using embedded PZT transducers in the A_0 mode demonstrates greater sensitivity for impact damage detection compared to surface-mounted PZT transducers at 50 kHz.

6. Conclusions

In summary, the paper investigated the effects of composite thickness on ultrasonic guided wave (UGW) behavior and damage detection using embedded PZT transducers. The active sensing results showed that the amplitude and group velocity of UGWs were influenced by the thickness of the composite panels, with a linear reduction observed as thickness increased. The temperature study revealed that the peak amplitude and time-of-flight (ToF) of UGWs were affected by temperature, with different behaviors observed depending on the thickness and mode. Comparisons between embedded and surface-mounted PZT transducers showed variations in the temperature responses, highlighting the advantages of using embedded PZT transducers in certain scenarios.

Damage detection and localization were performed for surface-mounted artificial damage and impact damage. The results demonstrated that both the A_0 and S_0 modes of UGWs could accurately detect and locate surface-mounted artificial damage. A comparison between embedded and surface-mounted results showed that the embedded PZT transducers had lower damage index values for the A_0 mode but higher values for the S_0 mode compared to surface-mounted PZT transducers. Additionally, the embedded PZT transducers exhibited better performance in locating surface-mounted artificial damage in thick composites, particularly at 250 kHz for the 9 mm panel.

For impact damage, the damage index and DAS algorithm successfully detected and located the damage using the A_0 mode at 50 kHz with embedded PZT transducers. The surface-mounted PZT transducers were not as effective in locating the impact damage. Overall, the results highlight the benefits of using embedded PZT transducers for UGW-based damage detection and localization, particularly in thick composite laminates. The findings provide valuable insights for the development of structural health monitoring systems and the optimization of damage detection techniques in composite structures.

Author Contributions: Experimental work, analysis and preparation of the manuscript, T.F.; supervision of research and preparation of the manuscript, M.H.F.A. All authors have read and agreed to the published version of the manuscript.

Funding: This research received no external funding. T. Feng's scholarship was funded by the Aviation Industry Corporation of China, Ltd. (AVIC), AVIC General Huanan Aircraft Industry Co., Ltd., and China Scholarship Council (No. [2017] 5082).

Institutional Review Board Statement: Not applicable.

Informed Consent Statement: Not applicable.

Data Availability Statement: Data sharing is not applicable.

Conflicts of Interest: The authors declare no conflict of interest.

References

1. Kahandawa, G.C.; Epaarachchi, J.; Wang, H.; Lau, K. Use of FBG sensors for SHM in aerospace structures. *Photonic Sens.* **2012**, *2*, 203–214. [[CrossRef](#)]
2. Giurgiutiu, V. *Structural Health Monitoring of Aerospace Composites*; Academic Press: New York, NY, USA, 2015.
3. Si, L.; Li, Z. Online structural state assessment for aerospace composite structures using an acousto-ultrasonics-based multi-damage index identification approach. *Struct. Health Monit.* **2020**, *19*, 1790–1807. [[CrossRef](#)]
4. Andreades, C.; Fierro, G.P.M.; Meo, M. A nonlinear ultrasonic SHM method for impact damage localisation in composite panels using a sparse array of piezoelectric PZT transducers. *Ultrasonics* **2020**, *108*, 106181. [[CrossRef](#)]
5. Marzani, A.; Testoni, N.; De Marchi, L.; Messina, M.; Monaco, E.; Apicella, A. An open database for benchmarking guided waves structural health monitoring algorithms on a composite full-scale outer wing demonstrator. *Struct. Health Monit.* **2020**, *19*, 1524–1541. [[CrossRef](#)]
6. Torkamani, S.; Roy, S.; Barkey, M.E.; Sazonov, E.; Burkett, S.; Kotru, S. A novel damage index for damage identification using guided waves with application in laminated composites. *Smart Mater. Struct.* **2014**, *23*, 095015. [[CrossRef](#)]
7. Liu, K.; Ma, S.; Wu, Z.; Zheng, Y.; Qu, X.; Wang, Y.; Wu, W. A novel probability-based diagnostic imaging with weight compensation for damage localization using guided waves. *Struct. Health Monit.* **2016**, *15*, 162–173. [[CrossRef](#)]
8. Wandowski, T.; Malinowski, P.; Ostachowicz, W. Circular sensing networks for guided waves based structural health monitoring. *Mech. Syst. Signal Process.* **2016**, *66*, 248–267. [[CrossRef](#)]
9. Yang, B.; Xuan, F.-Z.; Chen, S.; Zhou, S.; Gao, Y.; Xiao, B. Damage localization and identification in WGF/epoxy composite laminates by using Lamb waves: Experiment and simulation. *Compos. Struct.* **2017**, *165*, 138–147. [[CrossRef](#)]
10. Cantero-Chinchilla, S.; Chiachío, J.; Chiachío, M.; Chronopoulos, D.; Jones, A. A robust Bayesian methodology for damage localization in plate-like structures using ultrasonic guided-waves. *Mech. Syst. Signal Process.* **2019**, *122*, 192–205. [[CrossRef](#)]
11. Yang, B.; Xuan, F.Z.; Jin, P.; Hu, C.; Xiao, B.; Li, D.; Xiang, Y.; Lei, H. Damage Localization in Composite Laminates by Building in PZT Wafer Transducers: A Comparative Study with Surface-Bonded PZT Strategy. *Adv. Eng. Mater.* **2019**, *21*, 1801040. [[CrossRef](#)]
12. Muller, A.; Soutis, C.; Gresil, M. Image reconstruction and characterisation of defects in a carbon fibre/epoxy composite monitored with guided waves. *Smart Mater. Struct.* **2019**, *28*, 065001. [[CrossRef](#)]
13. Dafydd, I.; Khodaei, Z.S. Analysis of barely visible impact damage severity with ultrasonic guided Lamb waves. *Struct. Health Monit.* **2020**, *19*, 1104–1122. [[CrossRef](#)]
14. Memmolo, V.; Maio, L.; Boffa, N.D.; Monaco, E.; Ricci, F. Damage detection tomography based on guided waves in composite structures using a distributed sensor network. *Opt. Eng.* **2015**, *55*, 011007. [[CrossRef](#)]
15. Monaco, E.; Memmolo, V.; Boffa, N.; Maio, L.; Ricci, F. Guided waves based SHM systems: Parameters selection for better identification and localisation of damages in composites stiffened plates. In Proceedings of the Health Monitoring of Structural and Biological Systems 2017, Portland, UT, USA, 5 April 2017; p. 101701E.
16. Cantero-Chinchilla, S.; Aranguren, G.; Royo, J.M.; Chiachío, M.; Etxaniz, J.; Calvo-Echenique, A. Structural Health Monitoring Using Ultrasonic Guided-Waves and the Degree of Health Index. *Sensors* **2021**, *21*, 993. [[CrossRef](#)]
17. De Luca, A.; Caputo, F.; Khodaei, Z.S.; Aliabadi, M. Damage characterization of composite plates under low velocity impact using ultrasonic guided waves. *Compos. Part B Eng.* **2018**, *138*, 168–180. [[CrossRef](#)]
18. Dziendzikowski, M.; Kurnyta, A.; Dragan, K.; Klysz, S.; Leski, A. In situ Barely Visible Impact Damage detection and localization for composite structures using surface mounted and embedded PZT transducers: A comparative study. *Mech. Syst. Signal Process.* **2016**, *78*, 91–106. [[CrossRef](#)]
19. Lampani, L.; Sarasini, F.; Tirillò, J.; Gaudenzi, P. Analysis of damage in composite laminates with embedded piezoelectric patches subjected to bending action. *Compos. Struct.* **2018**, *202*, 935–942. [[CrossRef](#)]
20. Andreades, C.; Mahmoodi, P.; Ciampa, F. Characterisation of smart CFRP composites with embedded PZT transducers for nonlinear ultrasonic applications. *Compos. Struct.* **2018**, *206*, 456–466. [[CrossRef](#)]
21. Feng, T.; Sharif Khodaei, Z.; Aliabadi, M.H.F. Influence of Composite Thickness on Ultrasonic Guided Wave Propagation for Damage Detection. *Sensors* **2022**, *22*, 7799. [[CrossRef](#)]
22. Su, Z.; Ye, L. *Identification of Damage Using Lamb Waves: From Fundamentals to Applications*; Springer Science & Business Media: New York, NY, USA, 2009; Volume 48.

23. Andreades, C.; Malfense Fierro, G.P.; Meo, M.; Ciampa, F. Nonlinear ultrasonic inspection of smart carbon fibre reinforced plastic composites with embedded piezoelectric lead zirconate titanate transducers for space applications. *J. Intell. Mater. Syst. Struct.* **2019**, *30*, 2995–3007. [[CrossRef](#)]
24. Dziendzikowski, M.; Heesch, M.; Gorski, J.; Dragan, K.; Dworakowski, Z. Application of PZT Ceramic Sensors for Composite Structure Monitoring Using Harmonic Excitation Signals and Bayesian Classification Approach. *Materials* **2021**, *14*, 5468. [[CrossRef](#)] [[PubMed](#)]
25. Paget, C. Active Health Monitoring of Aerospace Composite Structures by Embedded Piezoceramic Transducers. Ph.D. Thesis, Department of Aeronautics, Royal Institute of Technology, Stockholm, Sweden, 2001.
26. Mall, S. Integrity of graphite/epoxy laminate embedded with piezoelectric sensor/actuator under monotonic and fatigue loads. *Smart Mater. Struct.* **2002**, *11*, 527. [[CrossRef](#)]
27. Matt, H.M. *Structural Diagnostics of CFRP Composite Aircraft Components by Ultrasonic Guided Waves and Built-in Piezoelectric Transducers*; University of California San Diego: San Diego, CA, USA, 2007.
28. Tuloup, C.; Harizi, W.; Aboura, Z.; Meyer, Y. Structural health monitoring of polymer-matrix composite using embedded piezoelectric ceramic transducers during several four-points bending tests. *Smart Mater. Struct.* **2020**, *29*, 125011. [[CrossRef](#)]
29. Lin, M.; Qing, X.; Kumar, A.; Beard, S.J. Smart layer and smart suitcase for structural health monitoring applications. In Proceedings of the Smart Structures and Materials 2001: Industrial and Commercial Applications of Smart Structures Technologies, Newport Beach, CA, USA, 14 June 2001; pp. 98–106.
30. Lin, M.; Chang, F.-K. The manufacture of composite structures with a built-in network of piezoceramics. *Compos. Sci. Technol.* **2002**, *62*, 919–939. [[CrossRef](#)]
31. Su, Z.; Wang, X.; Chen, Z.; Ye, L.; Wang, D. A built-in active sensor network for health monitoring of composite structures. *Smart Mater. Struct.* **2006**, *15*, 1939. [[CrossRef](#)]
32. Feng, T.; Aliabadi, M.H.F. Smart Patch for Structural Health Monitoring of Composite Repair. *Appl. Sci.* **2022**, *12*, 4916. [[CrossRef](#)]
33. Feng, T.; Bekas, D.; Aliabadi, M.H.F. Active Health Monitoring of Thick Composite Structures by Embedded and Surface-Mounted Piezo Diagnostic Layer. *Sensors* **2020**, *20*, 3410. [[CrossRef](#)]
34. Bekas, D.G.; Sharif-Khodaei, Z.; Aliabadi, M.H. An innovative diagnostic film for structural health monitoring of metallic and composite structures. *Sensors* **2018**, *18*, 2084. [[CrossRef](#)]
35. Feng, T.; Aliabadi, M.H.F. Structural Integrity Assessment of Composites Plates with Embedded PZT Transducers for Structural Health Monitoring. *Materials* **2021**, *14*, 6148. [[CrossRef](#)]
36. Yue, N.; Khodaei, Z.S.; Aliabadi, M.H. Damage detection in large composite stiffened panels based on a novel SHM building block philosophy. *Smart Mater. Struct.* **2021**, *30*, 045004. [[CrossRef](#)]
37. Zou, F.; Benedetti, I.; Aliabadi, M.H. A boundary element model for structural health monitoring using piezoelectric transducers. *Smart Mater. Struct.* **2013**, *23*, 015022. [[CrossRef](#)]
38. Yue, N.; Aliabadi, M.H. A scalable data-driven approach to temperature baseline reconstruction for guided wave structural health monitoring of anisotropic carbon-fibre-reinforced polymer structures. *Struct. Health Monit.* **2020**, *19*, 1487–1506. [[CrossRef](#)]
39. Michaels, J.E. Detection, localization and characterization of damage in plates with an in situ array of spatially distributed ultrasonic sensors. *Smart Mater. Struct.* **2008**, *17*, 035035. [[CrossRef](#)]
40. Sharif-Khodaei, Z.; Aliabadi, M. Assessment of delay-and-sum algorithms for damage detection in aluminium and composite plates. *Smart Mater. Struct.* **2014**, *23*, 075007. [[CrossRef](#)]

Disclaimer/Publisher’s Note: The statements, opinions and data contained in all publications are solely those of the individual author(s) and contributor(s) and not of MDPI and/or the editor(s). MDPI and/or the editor(s) disclaim responsibility for any injury to people or property resulting from any ideas, methods, instructions or products referred to in the content.